Sustainable Production and Consumption 60 (2025) 260–280

Contents lists available at ScienceDirect

Sustainable Production and Consumption

journal homepage: www.elsevier.com/locate/spc

Life cycle assessment of various agrivoltaic systems across Europe

Amirhossein Nik Zad [a,*], Alessandro Agostini [b], Giorgio Impollonia [a], Sebastian Zainali [c], Michele Croci [a], Michele Colauzzi [a], Pietro Elia Campana [c], Stefano Amaducci [a]

[a] Department of Sustainable Crop Production, Università Cattolica del Sacro Cuore, Piacenza, Italy
[b] ENEA–Italian National Agency for New Technologies, Energy and the Environment, Rome, Italy
[c] Department of Sustainable Energy Systems, Mälardalen University, Västerås, Sweden

ARTICLE INFO

Editor: Dr Kuishuang Feng

Keywords:
Agrivoltaic
Photovoltaic
Life cycle assessment
Environmental impacts
Monte Carlo Analysis
Climate change

ABSTRACT

The deployment of Conventional Ground-Mounted Photovoltaic (CGMPV) systems on farmland creates intense land-use competition with agriculture. Agrivoltaic (APVs) systems present a promising solution, yet the environmental viability of different designs remains insufficiently understood, hindering their strategic deployment. This study addresses this gap by presenting the first Life Cycle Assessment (LCA) benchmarking four bifacial APV systems, including fixed vertical, interspace, overhead single-axis, and overhead dual-axis systems with varying row pitch. These systems are compared against a bifacial CGMPV system (baseline scenario) and national electricity grid mixes, country-specific combinations of fossil, nuclear, and renewable sources, across north to south of Europe. A combined LCA method is applied, with attributional LCA evaluating PV components from cradle-to-end-of-use across ten impact categories, and a consequential approach addressing agricultural land-use change contributions to climate change category.

Results demonstrate that APV systems significantly outperform national electricity grids across nine impact categories, achieving 8–111 times lower environmental impacts. The interspace single-axis system emerged as the most optimal configuration with the lowest greenhouse gases (GHG) emissions (11–20 g CO_{2eq}/kWh), 57 % lower particulate matter, 48 % lower acidification, and 27 % lower eutrophication versus other APVs. The overhead dual-axis system showed the highest impacts (16–29 g CO_{2eq}/kWh), driven primarily by steel consumption in mounting structures. Monte Carlo Analysis confirmed that performance rankings are statistically robust. All APV systems showed 3.5–9.6 times higher mineral resource consumption than electricity grid mixes, highlighting a critical trade-off for sustainable resource management. These findings demonstrate that while APV systems can synergize food-energy systems with superior performance in most environmental categories, mineral resource intensity remains challenging, with material-efficient configurations essential for minimizing trade-offs.

1. Introduction

Agrivoltaic systems (APVs) enable simultaneous food and electricity production on the same land, offering improved land-use efficiency and renewable energy conversion while contributing to climate change mitigation. Unlike conventional single-use agricultural systems, which dedicate land exclusively to crop production without renewable energy integration, APVs represent a paradigm shift toward multifunctional land management (Weselek et al., 2019; Dinesh and Pearce, 2016a). However, this dual-use promise involves environmental trade-offs, including increased material consumption for mounting structures (particularly steel and aluminum), potential soil quality impacts from heterogeneous shading patterns, and altered water distribution affecting crop growth (Marrou et al., 2013; Amaducci et al., 2018). Life Cycle Assessment (LCA) provides essential quantification of these environmental impacts, guiding sustainable APV development. Despite growing research interest, current literature predominantly examines conventional fixed APV configurations with mono-facial photovoltaic (PV) modules, reflecting their commercial maturity and widespread deployment (Agostini et al., 2021; Wagner et al., 2023; Busch and Wydra, 2023). Advanced mounting structures and bifacial module technologies remain comparatively understudied, as illustrated in Fig. S1 in the Supporting Information (SI1), which shows the temporal distribution of LCA studies categorized by APV typologies and PV module types (Scopus database, 2014–2025, search terms: “LCA” AND (“agrivoltaics” OR “agro-photovoltaic” OR “agri-photovoltaic”)).

* Corresponding author.
E-mail address: amirhossein.nikzad@unicatt.it (A. Nik Zad).

https://doi.org/10.1016/j.spc.2025.10.003
Received 28 July 2025; Received in revised form 2 October 2025; Accepted 3 October 2025
Available online 8 October 2025

2. Literature review

2.1. Methodological approaches in APV life cycle assessment

LCA methodologies for APV systems demonstrate considerable heterogeneity in functional unit selection, system boundaries, and impact assessment methods. Functional units range from energy-based metrics (kWh_{el}), agricultural outputs (kg), land area (hectares), to economic indicators (revenue per hectare), each influencing result interpretation and comparability (Table S1 in SI1). System boundary definitions vary from cradle-to-gate assessments focusing on production phases to comprehensive cradle-to-grave analyses incorporating End-Of-Life (EOL) scenarios, though the latter remain uncommon, with most studies adopting cradle-to-end-of-use boundaries due to data limitations (Kiehbadroudinezhad et al., 2025). The allocation methodology for co-products significantly affects results. Leon and Ishihara (2018a) introduced a novel "solar allocation" method for greenhouse APV systems, demonstrating that system expansion yielded 0.83–0.95 kg CO_{2eq}/kg tomatoes, while economic allocation produced 0.98–1.10 kg CO_{2eq}/kg, representing approximately 15 % variation based solely on methodological choice. This methodological sensitivity underscores the importance of transparent reporting and sensitivity analysis in APV LCA studies.

2.2. Climate change mitigation performance

Regional-scale APVs deployment demonstrates substantial Greenhouse Gas (GHG) reduction potential. Implementation across 1–5 % of agricultural land in Baden-Württemberg, Germany, achieves annual reductions of 1.2–5.9 Mt. CO_{2eq}, with the upper range surpassing the region's entire agricultural sector emissions of ~4.4 Mt. $CO_{2Eq.}$ (Sponagel et al., 2024). System-specific performance varies considerably, with vertical bifacial configurations achieving 31–63 % lower climate change impacts compared to conventional agriculture combined with Austrian grid electricity (dominated by hydro and wind), while overhead fixed systems show a 36–70 % reduction in freshwater eutrophication and a 50–75 % reduction in fossil resource scarcity (Krexner et al., 2024). Greenhouse-integrated APV systems exhibit particularly strong mitigation potential. Integration with mushroom cultivation (*Panus giganteus*) reduces climate change impacts by 60 % (achieving 0.074–0.088 kg CO_{2eq}/kg product) compared to conventional production, while simultaneously decreasing freshwater eutrophication by 47 % and fossil depletion by 46 % (Cheng et al., 2024). Similarly, tomato greenhouse systems with organic PV achieved 12 % emission reduction through optimized solar allocation methodology (Leon and Ishihara, 2018b).

2.3. Material efficiency and system design optimization

Environmental performance correlates strongly with mounting structure design and material selection. Vertical bifacial APV systems consistently outperform overhead fixed configurations in a research study conducted in Austria, achieving lower environmental impacts across nine categories due to reduced steel and aluminum requirements, using glass-glass modules further enhances this advantage (Krexner et al., 2024). Comparative assessments of APV configurations in the United States revealed that APVs outperformed PV-only systems, achieving 15–55 % lower impacts per revenue dollar, with dual-axis tracking demonstrating optimal performance despite higher upfront costs (Ravilla et al., 2024). Balance-Of-System (BOS) components represent critical environmental hotspots. Steel mounting structures, zinc coatings, inverters, and copper cabling collectively contribute approximately to 80 % of non-module impacts across most APV configurations (Busch and Wydra, 2023; Ravilla et al., 2024). In Italy, tracking APVs achieved similar climate performance (~19–20 g CO_{2eq}/MJ) to ground-mounted PV (~22 g), substantially outperforming biogas (113–209 g) and grid electricity (~167 g), though the study notably excluded crop-side impacts and EOL considerations (Agostini et al., 2021).

2.4. Agricultural integration synergies

Integration strategies with different agricultural systems yield diverse sustainability outcomes. Livestock-integrated APVs demonstrate exceptional performance, with rabbit grazing systems achieving a 69.3 % reduction in GHG emissions and an 82.9 % decrease in fossil energy demand compared to spatially separated operations, primarily due to the elimination of feed production and transport (Pascaris et al., 2021). Sheep grazing configurations reduce emissions by 3.9 % compared to separated systems and achieve 280–894 % reduction versus grid electricity, with land-use efficiency doubling relative to separate operations (Handler and Pearce, 2022). Novel applications including data center integration with pasture-based APV in ecologically fragile regions demonstrate potential for over 3 Mt./year GHG reduction while restoring >1140 ha degraded land (Zhang et al., 2023). Crop-based systems exhibit variable performance correlating with shade tolerance. Consequential LCA of organic four-crop rotation in Germany showed environmental improvements in 15 of 16 categories, with particularly significant reductions in climate change (572.9 t CO_{2eq}/ha), freshwater eutrophication (524 kg P_{eq}/ha), and fossil resource use (6745 GJ/ha), though mineral resource use increased (+3.1 kg Sb_{eq}/ha) due to PV infrastructure (Wagner et al., 2023). Dynamic grape-voltaic models in India achieved up to 100 % elimination of groundwater by fully substituting irrigation needs with harvested rainwater, leading to substantial water savings (12–100 % reduction depending on the state), land savings of 1.984 ha/MW_p, and low carbon footprints (0.074–0.088 kg CO_{2eq}/kg grapes) through blockchain-enabled resource sharing (Kumar and Chopra, 2023).

2.5. Synthesis of current knowledge

Table S1 (SI1) synthesizes key LCA studies, revealing methodological diversity and highlighting critical knowledge gaps requiring investigation. Critical patterns emerge from this synthesis. First, functional unit selection profoundly influences comparability, studies using monetary units often show favorable results due to revenue stacking, while energy-based assessments enable direct comparison with conventional electricity. Second, regarding system boundaries, most studies (~85 %) employ either cradle-to-gate or cradle-to-end-of-use approaches, while only ~15 % include EOL phases. Notably, the few cradle-to-grave studies in literature have centered on mono-facial PV modules, offering only limited relevance for bifacial technologies. The present work employs a methodological scope consistent with the dominant body of LCA research on APVs, thereby allowing results to be positioned within a directly comparable framework. Third, geographic and climatic context strongly influence performance, yet most studies remain limited to single locations, underscoring the value of the multi-location assessment conducted in this study.

2.6. Research gaps and study contributions

Despite expanding LCA research on APVs, critical knowledge gaps persist. First, comparative assessments of multiple configurations within unified frameworks remain absent, limiting understanding of optimal design selection. Notably, no prior study has comprehensively compared vertical, single-axis, and dual-axis configurations equipped with bifacial PV modules. Second, detailed material inventories, particularly for vertical and tracking systems, are frequently withheld due to confidentiality agreements, hampering reproducibility and technology advancement. Third, environmental impact assessments disproportionately emphasize climate change while neglecting equally important categories including ecosystem quality and resource depletion. Fourth,

the integration of consequential and attributional LCA approaches remains underdeveloped, with most studies adopting single methodologies that fail to capture the complex interactions between energy conversion and agricultural systems.

This study addresses these gaps through comprehensive LCA benchmarking of four bifacial APV systems including fixed vertical, interspace and overhead single-axis, and overhead dual-axis configurations, against conventional ground-mounted bifacial PV systems and country-specific electricity grid mixes. The assessment spans diverse European climatic conditions from Sweden, Kärrbo Prästgård (59.55°N) to Italy, Agrigento (37.21°N), capturing latitudinal variation in solar resource availability and agricultural productivity patterns. The analysis employs a hybrid LCA methodology combining attributional assessment for PV components across ten environmental impact categories with consequential analysis for agricultural land-use change contributions to climate change. System boundaries explicitly encompass cradle-to-end-of-use phases, acknowledging the exclusion of EOL due to data limitations while maintaining consistency across all configurations. Critically, this research provides the first publicly available detailed material inventory for vertical APV systems. Monte Carlo Analysis ensures statistical robustness of conclusions. Through this comprehensive approach, the study identifies environmentally optimal APV configurations for sustainable food-energy co-production across European climatic gradients, providing actionable guidance for policymakers, developers, and agricultural stakeholders.

3. Methods

3.1. The study area and system description

To capture climatic variation across Europe, the study includes four geographically sites namely Kärrbo Prästgård in Sweden (59.5549°N, 16.7585°E), Jeggeleben in Germany (52.7305°N, 11.0285°E), and Piacenza (45.0524°N, 9.6923°E) and Agrigento (37.20920°N, 13.81800°E) in Italy, as illustrated in Fig. 1.

To ensure accurate and location-specific energy yield simulations, Typical Meteorological Years (TMYs) were constructed for each study site based on hourly reanalysis data from the ERA5 database (Hersbach et al., 2020), covering the period 2000–2024. Each TMY consisted of 8760 hourly values and was designed to represent long-term average

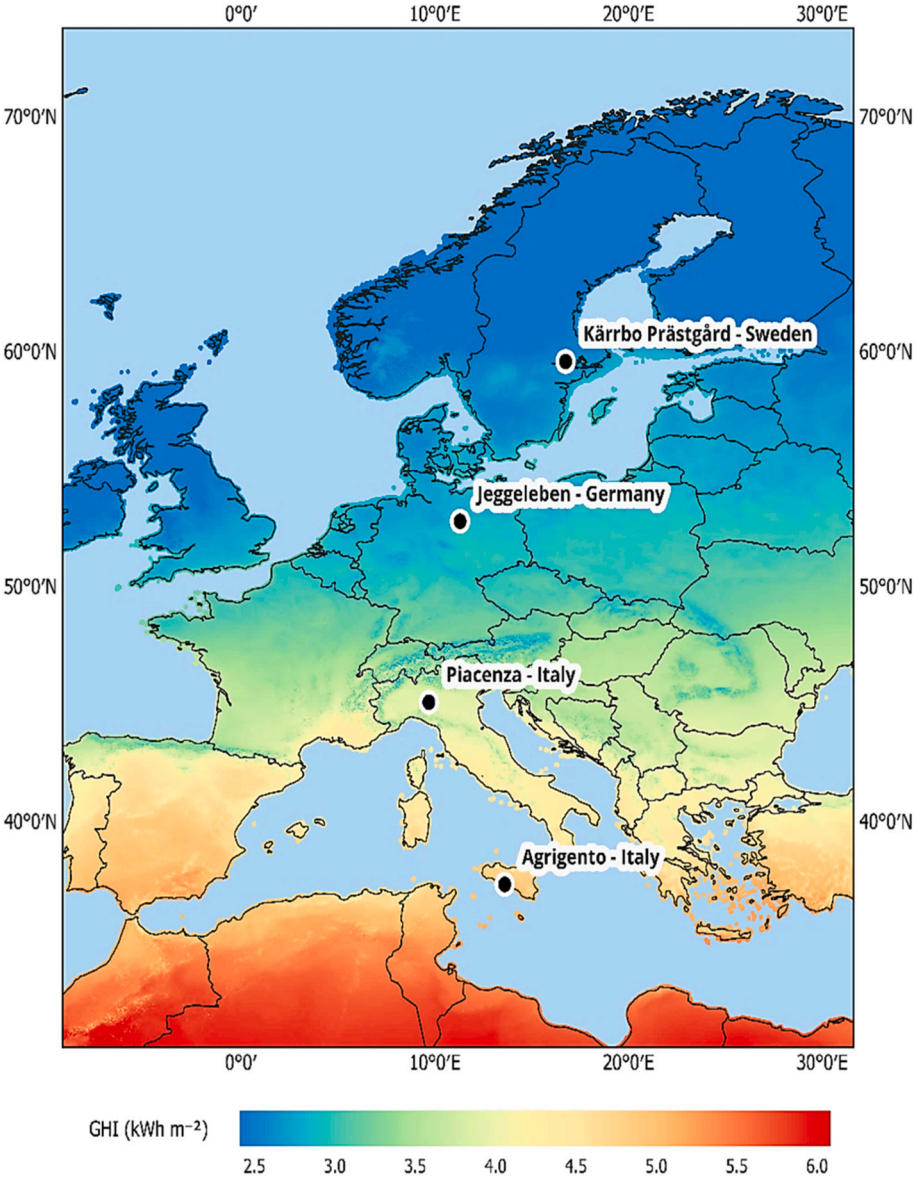

Fig. 1. Geographic locations analyzed in this study with average daily Global Horizontal Irradiance (GHI) values.

weather conditions while minimizing computational demand. The TMY construction followed the methodology established by the U.S. National Renewable Energy Laboratory (NREL) for TMY2 and TMY3 datasets (Wilcox and Marion, 2008) and conforms to ISO 15927-4:2005 standards (Kim et al., 2017). For each calendar month, all candidate months in the dataset were evaluated using the Finkelstein–Schafer (FS) statistic, which quantifies the deviation between a candidate month's Cumulative Distribution Function (CDF) and the long-term CDF. Daily values of Global Horizontal Irradiance (GHI), air temperature (T_a), and Relative Humidity (RH) were used as evaluation variables. A weighted FS score was computed for each candidate month, with weights of 60 % for GHI, 30 % for T_a, and 10 % for RH, reflecting their relative importance in PV performance modeling. The candidate month with the lowest weighted FS score was selected as most representative for each calendar month. These 12 months were then chronologically concatenated to create a synthetic year preserving intra-month weather patterns and irradiance variability. The resulting TMY datasets were used as standardized inputs for energy simulations (Fig. S2 in SI1).

This study examines four APV configurations, which include a fixed vertical system, an interspace single-axis setup, and two overhead tracking systems comprising single-axis and dual-axis mechanisms. These configurations reflect current industry standards and have been widely documented in previous research (Dupraz, 2023). The different systems are depicted in Fig. 2.

To establish fair performance comparisons, this study standardized the same PV module technology across all configurations. A 450 W_p bifacial module with 21.13 % efficiency and a 75 % bifaciality factor was selected. It weighs 29 kg, degrades by 0.5 % annually, and has a surface area of 2.13 m^2 (2.13 m × 1 m). A key decision was the selection of a representative, high-efficiency bifacial module, as this technology is central to modern APV systems (Riaz et al., 2022). Since Ecoinvent database lacks an inventory of bifacial PV module, this model was chosen based on the detailed Life Cycle Inventory (LCI) provided by Jia et al. (2021). The albedo was assumed to be 0.2, representing the fraction of global irradiation reflected from the ground onto the front and rear sides of bifacial modules (Nikzad and Mehregan, 2022). This value is commonly used as a baseline assumption in PV performance modeling for installations over vegetated or mixed ground surfaces (Johansson, 2023). While actual albedo may fluctuate depending on factors such as crop type, soil moisture, ground cover, and seasonal variations, the chosen value of 0.2 serves as a conservative and widely accepted average for generalized APV system simulations (Arthur et al., 2024; Zidane et al., 2025). The inverters used are three-phase, grid tied units operating at 50 Hz with an efficiency of 97.9 % (Huawei Technologies Co., 2025). Soiling and wiring losses were assumed to account for 2 % of the total system losses (Nikzad et al., 2019). The fixed vertical system had module rows aligned north-south, with vertically mounted modules (tilted 90°) facing east on one side and west on the other. The tracking systems also had north-south aligned rows and rotated from east to west to follow the sun's path, overhead single-axis trackers with a ± 55° rotation range and interspace single-axis trackers with a ± 45° range along the north-south axis. Dual-axis trackers rotated along both the north-south and east-west axes to fully track the sun. In contrast, the baseline system, Conventional Ground-Mounted Photovoltaic (CGMPV), had east-west aligned rows with modules facing north-south at a fixed tilt angle specific at each location. Each APV system type was analyzed under three different row pitches following the methodology outlined by Bellone et al. (2024), beginning from a baseline minimum spacing. A reduced pitch was allowed if it did not obstruct agricultural machinery or cause significant PV self-shading. To facilitate comparison across APV configurations, the three row pitch distances evaluated for each system, starting from the minimum feasible value, are referred to throughout the study as low, medium, and high pitch, respectively. The electricity output for a 1 MW_p capacity of each APV system and CGMPV at each location was simulated using PVSOL® software (PVSOL, 2024), with detailed results provided in SI2. Optimal tilt angles for the CGMPV system were also determined using the same software, resulting in values of 35° for Agrigento, 40° for both Piacenza and Jeggeleben, and 45° for Kärrbo Prästgård. Table 1 summarizes the layout and key design features of each system.

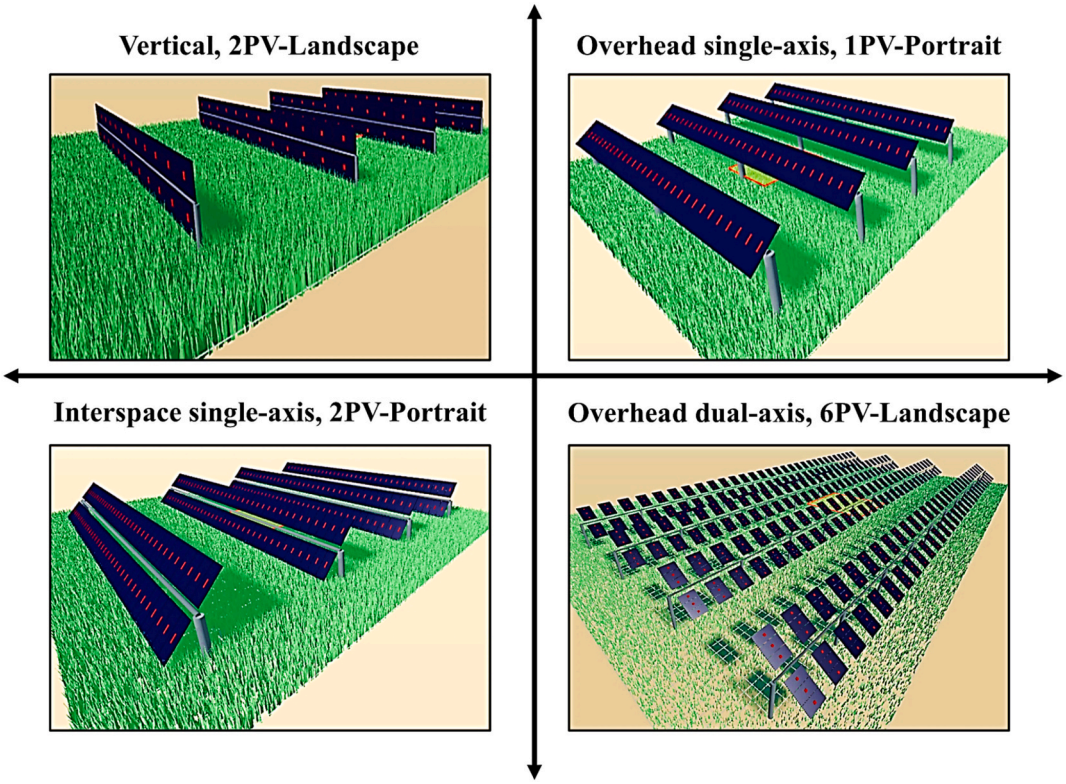

Fig. 2. Different APV layouts investigated in the present study.

Table 1
The settings of CGMPV and different APV systems used in this study.

APV type	Array layout	Height* (m)	Pitch (m)	Land use (ha/MW_p)
CGMPV (baseline)	2PV-Portrait	0.7	5	1.32
Fixed vertical	2PV-Landscape	0.7	8, 12, 16	1.95, 2.88, 3.82
Overhead single-axis	1PV-Portrait	2.8	6, 10, 14	1.44, 2.38, 3.34
Interspace single-axis	2PV-Portrait	2.3	10, 14, 18	1.21, 1.7, 2.16
Overhead dual-axis	6PV-Landscape	5	14, 18, 22	1.98, 2.48, 3.05

* In vertical system, the clearance from the ground to the bottom edge of the first PV panel is 70 cm. In tracking systems, this distance refers to the clearance from the hub to the ground.

3.2. Goal of the study

This study aims to evaluate the environmental impacts of different APV configurations across varied layouts and geographical settings spanning northern to southern Europe including Kärrbo Prästgård in Sweden, Jeggeleben in Germany, Piacenza and Agrigento in Italy as shown in Fig. 1. The objective is to improve understanding of their environmental performance during manufacturing and operation, supporting informed decision-making by farmers, industry stakeholders, and policymakers regarding optimal system selection for different regions.

3.3. Scope of the study

An attributional LCA is applied for the PV components of all APV systems, while the impact on agricultural production is assessed in terms of land losses by APV structures and shading-induced crop yield with a consequential LCA approach. The Functional Unit (FU) is 1 kWh of electricity conversion by various APVs. This choice aligns with the International Energy Agency (IEA) recommendation, which suggests it as a viable FU for solar PV-based systems (Nia et al., 2024).

The system boundary for PV systems follows an attributional cradle-to-end-of-use approach, encompassing raw material extraction, bifacial PV modules, mounting structures, inverters, tracking motors (where applicable), and electrical BOS components such as cables for each APV configuration. In contrast, the crop-related assessment adopts a consequential LCA framework and considers only the indirect land use impacts resulting from APV system deployment, which is discussed in detail later. The overall analysis spans 30 years, consistent with the expected lifetime of PV modules and structural components. Fig. 3 depicts the full system boundaries.

In this study, EOL phase for different systems, which involves dismantling the plant, waste processing, disposal, and recycling of all relevant plant components, were excluded due to the lack of sufficient and reliable information. This decision was made because the study focused solely on the construction and use phase. Although the EOL of PV modules can influence the LCA result, the modules used in all scenarios were identical, leading to the assumption that the EOL aspects would not significantly impact the comparison. This approach aligns with established methodologies in many LCA studies for APVs found in literature (Agostini et al., 2021; Busch and Wydra, 2023; Leon and Ishihara, 2018a; Leon and Ishihara, 2018b; Pascaris et al., 2021; Handler and Pearce, 2022).

3.3.1. Consequential impacts on crop production

Consequential crop impact is assessed using the Indirect Land Use Change (ILUC) method reported by Searchinger et al. (2008), which accounts for GHG emissions when APVs occupy arable land, potentially shifting crop production to other regions and increasing CO_2 emissions due to agricultural displacement (Agostini et al., 2021). ILUC emissions were estimated using the factor of 1595 kg CO_{2eq}/ha (Agostini et al., 2015), consistent with EU methodological guidelines. ILUC factors are derived from global economic and land use models (e.g., GLOBIOM, GTAP (Global economic model, 2025; Global land use model, 2025)) that simulate market-mediated land displacement and associated carbon stock changes. In this study, ILUC emissions were calculated as the product of excluded agricultural area and reduction/increase in crop productivity, the ILUC factor per hectare, and the project lifetime (30 years). While this static factor does not capture regional variability, it ensures methodological consistency. The arable land loss due to APV structures is calculated using a security buffer around APV mounting rows (support structures/trackers), representing the area excluded from cultivation for safe agricultural mechanization (Dinesh and Pearce,

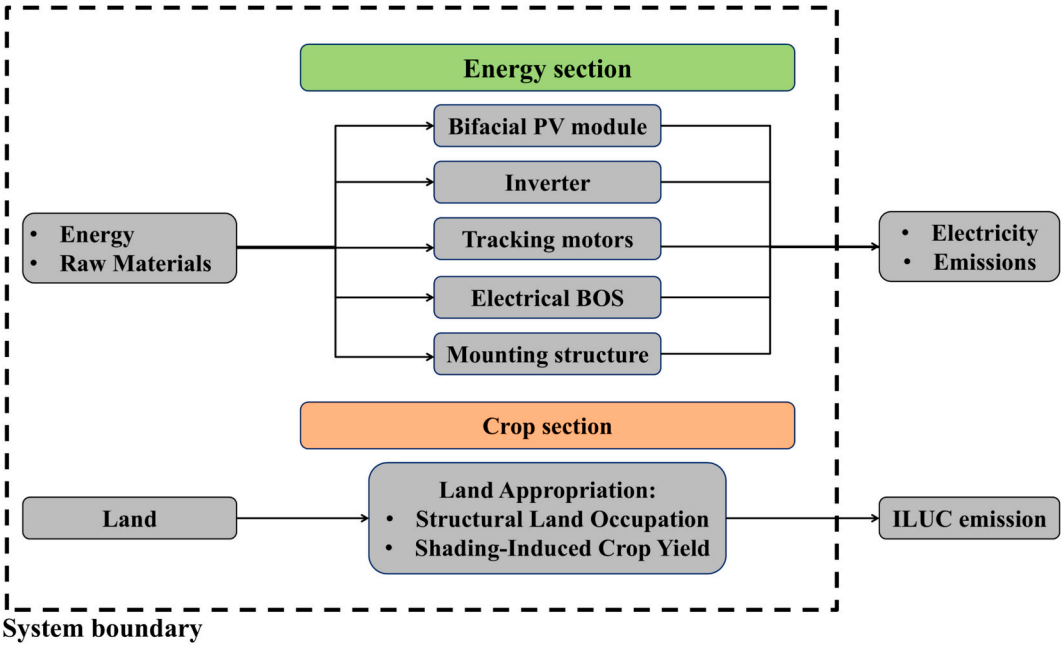

Fig. 3. System boundary of this research.

2016b). A 0.75-m buffer on both sides of each mounting row leads to the exclusion of 1.5 square meters of land per meter length of mounting row, accounting for the pillar diameter. The only exception applies to the interspace single-axis configuration, which uses a wider buffer of 1.5 m per side, resulting in 3 square meters of excluded land per meter of row. This exclusion is scaled according to the number of rows required to install 1 MW_p of capacity, yielding the total structurally non-cultivable land area. This area is then multiplied by the ILUC factor and the 30-year project lifetime to estimate the GHG emissions associated with permanent land occupation.

In addition to land exclusion caused by the APV structures, dynamic impacts on crop yield are also considered. Crop yield reductions can occur due to changes in the microclimate induced by APV structures, particularly reduced Photosynthetically Active Radiation (PAR). Unlike the previous factor, which quantified structural land occupation, this component captures dynamic yield penalties related to shading effects. To estimate crop yield reduction, a Multiple Linear Regression (MLR) model developed by Tekie et al. (2025) was adopted. This model was constructed from a meta-analysis of empirical yield data collected under APVs across various shading conditions. It includes five predictors: the shading level (X_1), and four climatic indicators (X_2: mean, X_3: minimum, X_4: maximum, X_5: standard deviation) derived from the Standardized Precipitation Evapotranspiration Index (SPEI), which together allow quantification of both light limitation and drought stress.

The shading predictor, X_1, was estimated using the irradiation model described by Amaducci et al. (2018), with hourly weather data from the ERA5 database (2000–2024), identical to that used for generating TMYs in the energy yield analysis, thereby ensuring methodological coherence. The model determined the annual reduction in GHI beneath the APV array compared to a Full Light (FL) reference scenario. To accurately account for the spatial heterogeneity in irradiation and potential edge effects beneath the PV arrays, shading was first calculated at a high spatial resolution of 0.5 m. This initial calculation encompassed the entire area between PV strings, capturing detailed light distribution patterns. From this high-resolution map, a single mean shading percentage, the required input for the subsequent yield estimation model, was derived by spatially averaging the values exclusively within the defined cultivated plot. The security buffer areas were deliberately omitted from this final averaging step to ensure the shading value accurately represented the conditions experienced by the crops and to avoid overestimation.

Climatic predictors (X_2–X_5) were derived from SPEI-1, a 1-month timescale index capturing short-term soil moisture variations. Monthly SPEI-1 values were calculated from the same weather dataset by modeling potential evapotranspiration via the Thornthwaite method and computing the climatic water balance (precipitation – PET). The resulting time series was fitted to a log-logistic distribution using the SPEI R package (Vicente-Serrano et al., 2010; Beguería et al., 2014) to standardize the drought indices. These predictors were parameterized on a basis specific to each crop. For each growing season, the four statistical moments were calculated using only the SPEI-1 data corresponding to that crop's defined growth cycle (X_2-X_5). This methodology accounted for the distinct phenological cycles of different crop types, including single-season annuals, winter crops with growth periods spanning two calendar years, and perennials for which a full 12-month period was considered. The MLR model was then used to estimate relative yield reduction as a function of shading and drought stress. The final set of calibrated MLR equations is reported in Table 2 for seven non-irrigated crop categories.

These equations allow direct integration of shading–climate interactions into APVs planning, enabling context-specific yield reduction assessments. Additional details on model structure, accuracy, and validation are provided by Tekie et al. (2025). Once relative yield reductions are estimated, the associated emissions are calculated by multiplying the percentage yield loss by the net cultivable area (excluding the security buffer areas), the ILUC factor, and the project lifetime. As the ILUC factor is defined on a per-hectare basis and not crop-specific, yield losses are interpreted as land-equivalent losses. For instance, a 20 % reduction in crop yield is considered equivalent to a 20 % reduction in productive land area. This assumption allows for the integration of shading-induced productivity losses into a land-based emission framework in a methodologically consistent and reproducible manner, in line with the principles of consequential LCA. Conversely, in cases where crop yield under the APVs improves due to the adoption of shade-tolerant crops or favorable microclimatic conditions, a credit is assigned using the same methodological approach. The resulting gain in yield is interpreted as an equivalent increase in productive land area and leads to negative ILUC emissions, reflecting the avoided land use that would otherwise be required to achieve the same level of agricultural output. Finally, the GHG emissions resulting from the consequential approach were combined with the GHG emissions associated with attributional approach. To ensure consistency with the study's functional unit (kWh), the total emissions were normalized by the cumulative electricity generation of each 1 MW_p APV configuration at each location over the system's lifetime. The resulting values were then assigned to the climate change impact category within the LCA framework.

Table 2
Regression equations derived from the MLR models for non-irrigated crop categories (Tekie et al., 2025).

Crop type	Equations
C3 Cereals	$Y = 71.34 - 0.76X_1 + 5.84X_2 + 12.47X_3 - 8.01X_4 + 67.09X_5$
Berries	$Y = 111.58 + 0.021X_1 - 16.78X_2 - 7.84X_3 - 50.16X_4 + 70.31X_5$
Maize	$Y = 86.84 - 0.47X_1 + 58.21X_2 - 9.55X_3 - 46.76X_4 + 49.29X_5$
Grain Legumes	$Y = 126.25 - 0.87X_1 - 37.61X_2 + 48.93X_3 - 5.39X_4 + 38.47X_5$
Fruits	$Y = 107.06 - 0.42X_1 + 6.52X_2 - 5.42X_3 - 2.22X_4 - 5.94X_5$
Root crop	$Y = 20.59 - 0.81X_1 - 26.50X_2 - 17.96X_3 - 22.61X_4 + 84.89X_5$
Forage	$Y = 78.68 - 0.93X_1 + 86.36X_2 - 31.22X_3 - 64.20X_4 + 123.21X_5$

*Y indicates the predicted crop yield (% of reference yield).

3.4. Life Cycle Inventory (LCI)

Ecoinvent v3.8 datasets (Ecoinvent, 2021) were used to model all system components, excluding PV modules, for the APV configurations and the country-specific electricity grid mix (electricity, medium voltage (Busch and Wydra, 2023)). Detailed national electricity mix compositions are provided in Fig. S3 (SI1). The analyses were conducted using the allocation, cut-off by classification system model, which is consistent with standard practice for attributional LCA (Steubing et al., 2016). Since the studied systems are not modeled as multifunctional (the functional unit is defined as 1 kWh of electricity), no additional allocation procedures were required. As this Ecoinvent database does not include a dedicated dataset for bifacial PV modules, a new process was created within the SimaPro® software to model the selected 450 W_p module. The inventory for this process was adapted from the study by Jia et al., (2021). Specifically, the material and energy inputs were derived from their inventory for the "166-BF (72)" module, which corresponds to a 450 W_p bifacial module. The data reported by Jia et al., (2021) is normalized per 1 kW_p of capacity; therefore, all values were scaled by a factor of 0.45 to accurately represent the inputs for a single 450 W_p module. The resulting inventory is detailed in Table 3.

For the CGMPV system, the Ecoinvent dataset was modified to align with the selected bifacial PV module technology and to standardize the configuration to a 1 MW_p capacity over a 30-year project lifetime. These adjustments ensure a consistent basis for fair comparison with the APV configurations in terms of system design and energy yield. The default PV modules in the Ecoinvent dataset were replaced with the custom-modeled 450 W_p bifacial modules used in the APV systems. The inverter inventory was revised to include two 500 kW_p inverters and one replacement at year 15, reflecting a more realistic operational lifetime (Ravilla et al., 2024) and resulting in four units over the system lifespan. The BOS inventory was proportionally scaled from the Ecoinvent dataset

Table 3
Life cycle inventory for a single 450 W_p Bifacial PV Module. Data adapted from (Jia et al., 2021).

Materials	Life Cycle Stage	Flow Type	Units	Values	Remarks
Silicon wafer	Cell Manufacturing	Input	kg	0.833	Silicon, single crystal, Czochralski process, photovoltaics (RoW) | market for |
Metallization paste, back side	Cell Manufacturing	Input	kg	0.0107	Metallization paste, back side (RoW) | market for |
Metallization paste, back side, Aluminum	Cell Manufacturing	Input	kg	0.0107	Metallization paste, back side, aluminum (RoW) | market for |
Metallization paste, front side	Cell Manufacturing	Input	kg	0.0107	Metallization paste, front side (RoW) | market for |
HF	Cell Manufacturing	Input	kg	0.6484	Hydrogen fluoride (RoW) | market for |
HNO_3	Cell Manufacturing	Input	kg	0.6484	Nitric acid, without water, in 50 % solution state (RoW) | market for |
HCI	Cell Manufacturing	Input	kg	0.6484	Hydrochloric acid, without water, in 30 % solution state (RoW) | market for |
H_2SO_4	Cell Manufacturing	Input	kg	0.6484	Sulfuric acid (RoW) | market for |
KOH	Cell Manufacturing	Input	kg	0.6484	Potassium hydroxide (GLO) | market for |
H_2O_2	Cell Manufacturing	Input	kg	0.6484	Hydrogen peroxide, without water, in 50 % solution state (RoW) | market for |
O_2	Cell Manufacturing	Input	kg	0.6484	Oxygen, liquid (RoW) | market for |
NH_3	Cell Manufacturing	Input	kg	0.6484	Ammonia, liquid (RoW) | market for |
$POCI_3$	Cell Manufacturing	Input	kg	0.6484	Phosphorus oxychloride (GLO) | market for |
N_2	Cell Manufacturing	Input	kg	0.6484	Nitrogen, liquid (RoW) | market for |
POE	Module Assembly	Input	kg	2.376	Polyolyaltha Olfin, replaced by Polyethylene, low density, granulate (GLO) | market for |
Ribbons	Module Assembly	Input	kg	0.212	Copper (GLO) | market for |
Solar glass	Module Assembly	Input	kg	21.281	Solar glass, low - iron (GLO) | market for |
Aluminum frame	Module Assembly	Input	kg	2.3	Aluminum alloy, AlMg3 (GLO) | market for |
Tap water	Cell & Module Manufacturing	Input	kg	188.28	Tap water (RoW) | market for |
Electricity	Cell & Module Manufacturing	Input	kWh	24.503	Electricity, low voltage | market group for |

of a 570 kW_p electrical and mounting installation, using a scaling factor of 1.754 to represent a 1 MW_p system. PV modules and mounting structures were assumed to have a lifespan of 30 years, in line with the project lifetime (Jia et al., 2021; Mason et al., 2006).

Table 4 presents the aggregated component inventories for electricity generation in both CGMPV and APV systems, standardized to a 1 MW_p capacity over the 30-year lifetime.

It is important to highlight that the material inventories used, particularly those related to tracking motors and structural BOS components for the different APV configurations, were obtained through direct personal communication with industry sources. These inventories may vary across manufacturers due to proprietary designs, patented innovations, and differences in structural design and material composition. In particular, some systems may employ lighter or heavier support structures (trackers) or utilize materials with higher or lower environmental impacts. Such variations can significantly influence LCA results and should be carefully considered when generalizing findings across different APV technologies. The structural design of each APV followed a specific commercial reference including Agrivoltaico Tracker 3D-T2.1 for the dual-axis system (REM TEC® (REM TEC S.R.L., 2025)), CONVERT TRJ15 for the overhead single-axis system (Valmont Solar® (Valmont Solar, 2025)), CONVERT TRJ72 for the interspace single-axis configuration (Valmont Solar, 2025), and SkyGre P2-DUO for the vertical system (SentNet® (SentNet S.R.L., 2025)). Table 5 details the technical specifications of the fixed vertical and tracking APVs, as provided by industry partners for the life cycle inventories. These specifications formed the basis for the estimation of material and energy flows. All inventories were scaled to a uniform system size of 1 MW_p to ensure comparability.

Finally, the inventory of all material used was modeled using SimaPro® software (SimaPro, 2025), a leading software for LCA calculations (Chavez et al., 2025).

3.5. Life Cycle Impact Assessment (LCIA)

The Environmental Footprint (EF) method recommended by the International Life Cycle Data (ILCD) System (Fazio et al., 2018) was adopted for assessing environmental impacts in this study. This method translates life cycle inventory data into quantitative contributions to specific environmental concerns. An EF impact category denotes a particular type of resource use or environmental impact associated with the life cycle inventory data, and each impact category is represented by a quantifiable indicator. Although the EF method defines 16 impact categories, the present study selected 10 of them. This selection was guided by their methodological robustness, consistency with previous scientific literature on APVs (Agostini et al., 2021), and alignment with recommendations provided by the European Commission guidelines

Table 4
Aggregated life cycle inventory of material inputs for 1 MW_p capacity of CGMPV and four APV typologies, over a 30-year lifetime.

Components	Materials	Units	CGMPV (2P)	Fixed vertical (2 L)	Overhead single-axis (1P)	Interspace single-axis (2P)	Overhead dual-axis (6 L)	Dataset and References
PV module	Bifacial photovoltaic panel, single-Si, 450 W_p	Pieces	2223	2223	2223	2223	2223	(Jia et al., 2021)
Inverter	Inverter 500 kW_p	Pieces	2 + 2	2 + 2	2 + 2	2 + 2	2 + 2	Ecoinvent, Inverter 500 kW_p (GLO) | market for | (Ecoinvent, 2021)
Tracking motor	Steel, copper, plastic	kg	–	–	621	391	650	Ecoinvent, Electric motor, vehicle (GLO) | market for | (Ecoinvent, 2021; Valmont Solar, 2025; SentNet S.R.L., 2025)
Wiring	Copper, plastic	kg	Included in Ecoinvent dataset	1300	2710	2445	2950	Ecoinvent, Cable (GLO) | market for | (Agostini et al., 2021; Busch and Wydra, 2023; Méndez et al., 2021) Ecoinvent, Electric installation, for CGMPV (GLO) | market for | (Ecoinvent, 2021)
Structural BOS			Included in Ecoinvent dataset					Ecoinvent, Photovoltaic mounting system, for CGMPV (GLO) | market for | (Ecoinvent, 2021)
	Steel	kg	–	60,000	114,108	53,785	236,158	Ecoinvent, Reinforcing steel (GLO) | market for | (REM TEC S.R.L., 2025; Valmont Solar, 2025; SentNet S.R.L., 2025)
	Aluminum	kg	–	140	227	171	7.15	Ecoinvent, Aluminum, wrought alloy (GLO) | market for | (REM TEC S.R.L., 2025; Valmont Solar, 2025; SentNet S.R.L., 2025)
	Zinc	kg	–	2100	4021	2690	3900	Ecoinvent, Zinc (GLO) | market for | (REM TEC S.R.L., 2025; Valmont Solar, 2025; SentNet S.R.L., 2025)

Table 5
Key technical specifications of the vertical and tracking APV systems.

	Fixed vertical (2 L)	Overhead single-axis (1P)	Interspace single-axis (2P)	Overhead dual-axis (6 L)
Number of PV modules per support structure/tracker	24	15	72	18
Total PV capacity per support structure/tracker (kW_p)	10.8	6.75	32.4	8.1
Total number of support structures/ trackers required/1 MW_p	93	148	31	124
Length of each support structure/tracker (m)	26	18	41	10.5

Table 6
EF impact categories and their corresponding indicators used in this study.

Impact category	Indicator	Unit
Climate change	Global Warming Potential (GWP100)	g $CO_{2\ eq}$
Ozone depletion	Ozone Depletion Potential (ODP)	*µg CFC-11 $_{eq}$
Respiratory inorganics (Particulate matter)	Impact on human health	Disease incidence
Photochemical Ozone formation	Tropospheric ozone concentration increase	**mg NMVOC $_{eq}$
Acidification	Accumulated Exceedance (AE)	mmol $H+_{\ eq}$
Eutrophication, terrestrial	Accumulated Exceedance (AE)	mmol $N_{\ eq}$
Eutrophication, freshwater	Fraction of nutrients reaching freshwater end compartment (P)	mg $P_{\ eq}$
Eutrophication, marine	Fraction of nutrients reaching marine end compartment (N)	mg $N_{\ eq}$
Resource use, minerals and metals	Abiotic resource depletion (ADP ultimate reserves)	mg $Sb_{\ eq}$
Resource use, fossils	Abiotic resource depletion – fossil fuels (ADP-fossil), Uranium is included	MJ

* CFC-11 = Trichlorofluoromethane.
** NMVOC = Non-Methane Volatile Organic Compounds.

(Fazio et al., 2018). Table 6 summarizes the selected EF categories, and their corresponding indicators used in this study.

3.6. Uncertainty analysis in LCIA

The uncertainty analysis aimed to quantify the influence of background data variability on the results across all impact categories for APV systems. It considered two distinct components. The first was the background processes, which were modeled as stochastic variables using Ecoinvent v3.8 "market for" datasets with global (GLO) coverage, as detailed in Table 4. These background flows were treated as stochastic, characterized by lognormal uncertainty distributions inherent to the database. Specifically, the uncertainty for these background processes, particularly for emissions and resource inputs, was estimated using the Pedigree matrix approach. This methodology, integrated within SimaPro and explained in its official documentation, assesses the data quality of each background data point based on six criteria including reliability, completeness, temporal correlation, geographical correlation, technological correlation, and a basic uncertainty factor (Weidema and Wesnæs, 1996). The overall squared geometric standard deviation σ^2 for each data point's uncertainty, which defines the spread of its lognormal distribution, is calculated as follows:

$$\sigma^2 = \sum_{n=1}^{6} \sigma_n^2 \quad (1)$$

The second component was the foreground data, referring to the quantities of materials and components used in each APV configuration.

These were treated as deterministic values and were primarily derived from direct communication with industry sources. While no probability distributions were assigned to these values, they were included in the Monte Carlo Analysis alongside the background data to preserve model consistency. To perform the uncertainty analysis, a Monte Carlo Analysis was executed using SimaPro's built-in functionality. This simulation, carried out for 10,000 iterations, randomly sampled values from the defined probability distributions, including those determined by the Pedigree matrix for background data. The resulting uncertainty was expressed as 95 % confidence intervals, indicating the statistical range within which the true mean value is expected to lie with 95 % probability. For a more detailed explanation of the Pedigree matrix and uncertainty calculation methods within SimaPro, readers are referred to the software's official introduction manual (SimaPro, 2025).

4. Results

4.1. GHG emissions caused by structural land occupation

Understanding how APV infrastructure affects agricultural land availability is essential for evaluating system sustainability. The structural footprint of each configuration was quantified to estimate non-cultivable land area and its corresponding GHG emissions using the ILUC method, as summarized in Table 7. These values represent a consequential component of the LCA, highlighting how design choices influence environmental trade-offs between clean energy conversion and land preservation.

The results reveal significant design-dependent variability. The overhead dual-axis system was the most land-efficient, occupying only 1953 m^2/MW_p (Bellone et al., 2024) and generating the lowest lifetime emissions (9.35 t CO_{2eq}). In contrast, the overhead single-axis configuration had the largest non-cultivable footprint at 3996 m^2/MW_p (Bellone et al., 2024) and, consequently, the highest emissions (19.12 t CO_{2eq}). This was primarily due to its lower module density, which necessitated the highest number of trackers per MW_p (Bellone et al., 2024). The fixed vertical (3627 m^2/MW_p) and interspace single-axis (3813 m^2/MW_p) systems demonstrated intermediate performance (Bellone et al., 2024), with the latter showing a modest 4.8 % reduction in non-cultivable area compared to the overhead single-axis design, despite having a much longer structural length. These findings on the contribution of APV structural land occupation to the ILUC-related GHG emissions represent one component that should be integrated with other factors, including the GHG impacts from crop yield variations and the emissions from PV component materials in each APV configuration. Only after this comprehensive integration and normalization per FU can a conclusive LCA benchmark the overall environmental performance of the various APV systems.

Table 7
Consequential GHG emissions of structural land occupation of 1 MW_p APV systems.

APV system type	Fixed vertical (2 L)	Overhead single-axis (1P)	Interspace single-axis (2P)	Overhead dual-axis (6 L)
Total non-cultivable area per 1 MW_p (m^2)	3627	3996	3813	1953
ILUC-related GHG emissions for non-cultivable area per 1 MW_p ($kgCO_{2eq}$)	578.5	637.4	608.2	311.5
ILUC-related GHG emissions over 30-year project lifetime ($tonCO_{2eq}$)	17.35	19.12	18.47	9.35
Pitch	8 m/12 m/16 m	6 m/10 m/14 m	10 m/14 m/18 m	14 m/18 m/22 m
Total land area required per 1 MW_p (ha)	1.95/2.88/3.82	1.44/2.38/3.34	1.2/1.7/2.16	1.98/2.48/3.05
Net cultivable land area available per 1 MW_p (ha)	1.59/2.52/3.46	1.04/1.98/2.94	0.83/1.32/1.78	1.78/2.28/2.85

4.2. GHG emissions caused by crop yield variations

Evaluating how different APV system designs influence crop yields is essential to understanding their broader environmental impacts. Fig. 4 illustrates the GHG emissions associated with crop yield variations under APV configurations for each location at medium pitch spacing across the selected crops in this study. A reduction in yield leads to increased GHG emissions due to the need for compensatory production elsewhere, while an increase in yield results in GHG savings by offsetting production in other regions (Agostini et al., 2021; Sponagel et al., 2024). Results for lower and upper pitches are provided in SI2.

Among tracking APV systems, a consistent trend emerges across crops and locations, with root crops demonstrating the highest ILUC-related GHG emissions due to their pronounced sensitivity to shading-induced yield reduction. Conversely, berries consistently deliver substantial GHG emission savings (credits), attributable primarily to their inherent shade tolerance. Cereals, maize, grain legumes, fruits, and root crops all experience their highest yield-induced GHG emissions in the overhead dual-axis APV system, consistent with broader assessments that associate APV design choices with climate impacts (Sponagel et al., 2024). Despite the interspace design having higher shading levels at all locations, resulting from its lower height and the use of two PV modules instead of one in portrait orientation, it consistently shows lower ILUC-related GHG emissions and credits compared with the overhead single-axis system. For example, in Piacenza, the shading level for the interspace single-axis system was calculated at 26 %, whereas the overhead single-axis system showed 21.52 %. The significantly smaller net cultivable land area remaining available per MW_p installed capacity (approximately 50 %) for the interspace system, compared to the overhead counterpart, ultimately led to lower ILUC-related GHG emissions and credits (Agostini et al., 2021; Sponagel et al., 2024). The vertical APV system exhibits a similar general pattern, with root crops again recording the highest ILUC-related GHG emissions, reflecting their heightened shade sensitivity under medium pitch spacing across all APV configurations. However, for fruits and grain legumes, overall positive GHG emission contributions are observed, driven by yield enhancements at shading levels of up to 14 %. Specifically, fruit yields improved at all locations, whereas grain legumes exhibited yield increases in most locations except Kärrbo Prästgård and Jeggeleben. In contrast to the tracking systems where berries delivered the highest GHG emission savings, forage crops within the vertical APV system consistently demonstrated the greatest emission reductions across all locations. Specifically for forage within the vertical APV system, which recorded the highest ILUC-related GHG credits among all APV configurations, Agrigento showed the greatest yield increase (+30.2 % relative to open-field condition), followed by Kärrbo Prästgård (+25.8 %), Piacenza (+23.8 %), and Jeggeleben (+22.1 %). Detailed data on shading levels and yield variations across locations and APV configurations at various pitches are provided in SI2. These findings will be integrated with GHG emissions from APV structural land occupation as well as materials used in PV components. The normalization process, detailed in Section 4.4.1, will be applied following this integration to ensure comprehensive assessment and enable conclusive interpretation of environmental impacts.

4.3. GHG emission contribution of PV components

Fig. 5 depicts the GHG emissions associated with the electrical and structural material inputs across APV configurations. The emissions

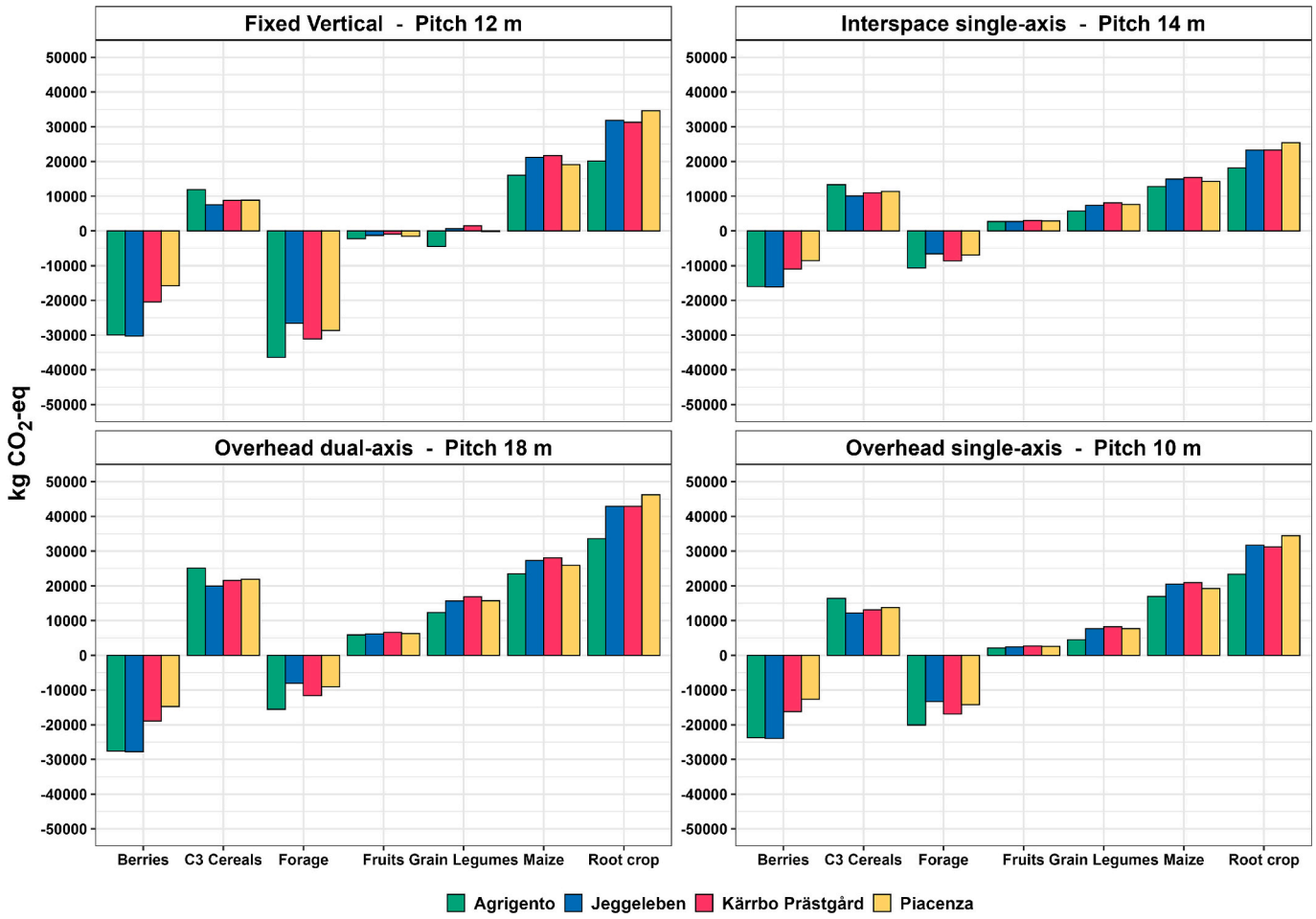

Fig. 4. GHG emissions and credits associated with crop yield variation under medium pitch APV configurations across crop groups and locations.

provide a detailed breakdown for key PV components such as PV modules, inverters, tracking motors, wiring and structural BOS.

The results demonstrate a clear correlation between system complexity and material-related emissions. The overhead dual-axis system had the highest emissions at 1151.8 t CO_{2eq}, a full 55 % higher than the least impactful design. This was driven by its substantial steel requirement of 236.2 tons, needed to support a 5-m installation height. The interspace single-axis configuration was the best performer (742.8 t CO_{2eq}), benefiting from a reduced height (2.3 m) that required only 53.8 tons of steel. The fixed vertical system (747.1 t CO_{2eq} from 60 tons of steel) and the overhead single-axis system (884.9 t CO_{2eq}) had intermediate emissions. The overhead single-axis design produced about 19 % more emissions than the interspace system, consistent with its moderate structural requirements at a height of 2.8 m. Emissions from bifacial PV modules (485.8 t CO_{2eq}) and inverters (111.9 t CO_{2eq}) were constant across all configurations, while tracking motors added a smaller contribution of 1.5–2.6 t CO_{2eq} depending on the system. This pattern corroborates the trends reported in prior studies (Agostini et al., 2021; Sponagel et al., 2024).

4.4. Overall environmental impact assessment

In this section, all impact categories listed in Table 6 are assessed across all APV configurations compared to the baseline system (CGMPV) and country-level electricity grid mix at all locations at medium pitch spacing, with all systems normalized per functional unit for fair comparison. It should be noted that increasing row pitch reduces GHG emissions per kWh. This effect is due to minimizing near-shading losses between PV strings, which in turn improves the overall electricity conversion efficiency (Bellone et al., 2024). Consequently, with a fixed material inventory for a given capacity, a higher energy output effectively dilutes the life cycle impacts when normalized by the FU (kWh). The complete numerical results for all impact categories across all systems, locations and pitches are provided in SI2.

4.4.1. Climate change

Assessing climate impacts across system types and regions provides insight into the decarbonization potential of APVs. Fig. 6 presents the normalized GHG emissions across different APV configurations, crop groups, and locations, alongside comparisons with the country-specific electricity grid mix and CGMPV system.

The interspace single-axis system consistently demonstrates the lowest GHG emissions across all locations and crop types (11.2–19.8 g CO_{2eq}/kWh). The overhead dual-axis system consistently exhibits the highest GHG emissions per unit of electricity across all locations and crop types (16.3–29.1 g CO_{2eq}/kWh). The fixed vertical system depicts the second highest emissions (15.8–27.5 g CO_{2eq}/kWh), exceeding those of the interspace single-axis design (Sponagel et al., 2024). The overhead single-axis system shows intermediate emissions (13.1–23.4 g CO_{2eq}/kWh), reflecting moderate structural requirements and additional tracking components compared to the fixed vertical system.

A pronounced geographic trend emerges across all system types, with Agrigento consistently yielding the lowest GHG emissions per kWh, followed by Piacenza, Jeggeleben, and Kärrbo Prästgård. Under the interspace single-axis configuration, Agrigento achieves the lowest observed emission value for berries (11.2 g CO_{2eq}/kWh), while the same

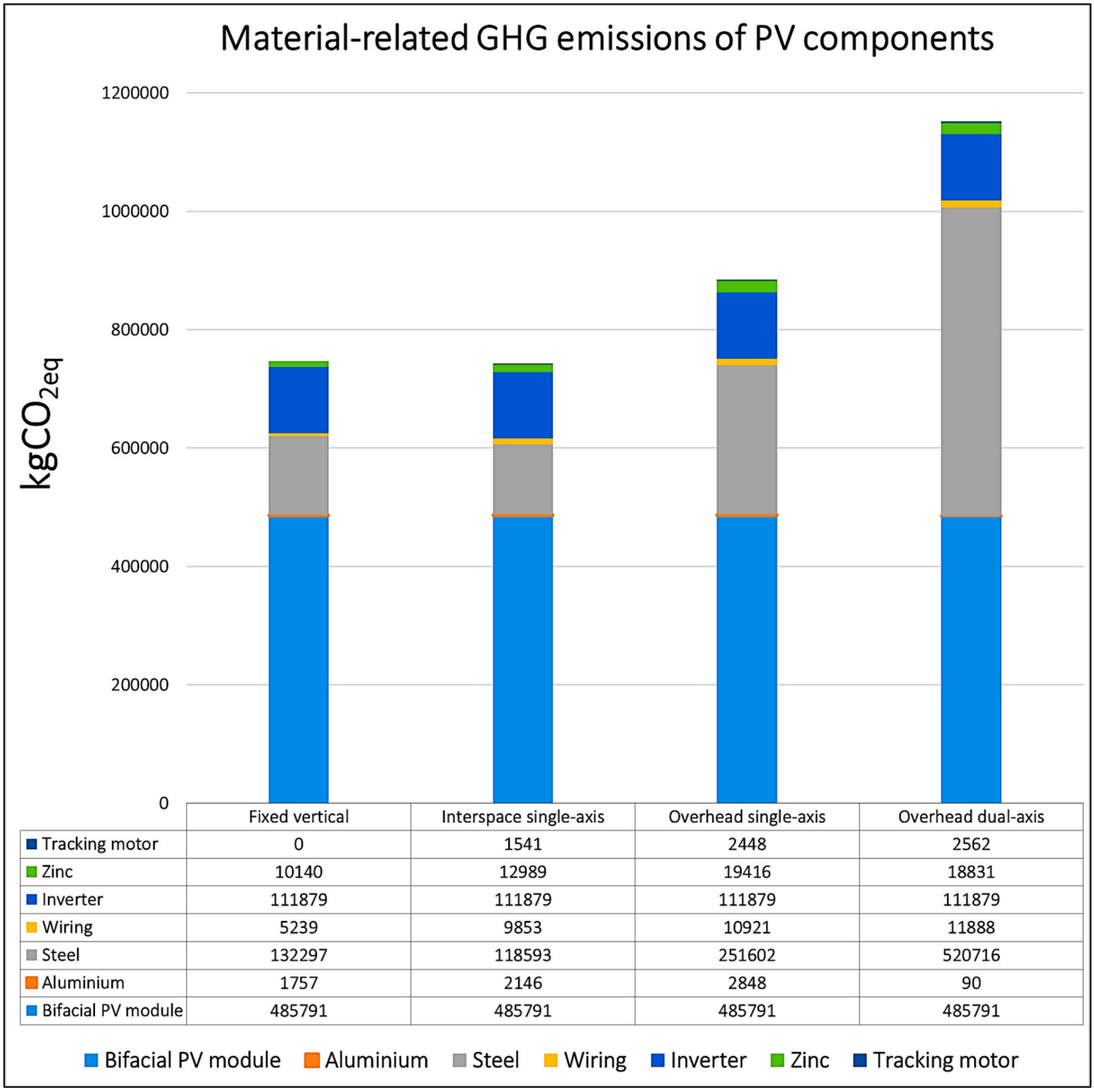

	Fixed vertical	Interspace single-axis	Overhead single-axis	Overhead dual-axis
Tracking motor	0	1541	2448	2562
Zinc	10140	12989	19416	18831
Inverter	111879	111879	111879	111879
Wiring	5239	9853	10921	11888
Steel	132297	118593	251602	520716
Aluminium	1757	2146	2848	90
Bifacial PV module	485791	485791	485791	485791

Fig. 5. GHG contributions of PV component materials for various APV systems, calculated per 1 MW_p.

system for the same crop type in Kärrbo Prästgård emits nearly 19 g CO_{2eq}/kWh due to significantly lower solar intensity.

APV structural land occupation has a relatively minor influence on overall climate change results. The variations range from a minimum of 0.13 g CO_{2eq}/kWh in Agrigento for dual-axis APV systems to a maximum of 0.62 g CO_{2eq}/kWh in Kärrbo Prästgård for fixed vertical APV systems. The differences among crop types also have relatively minor influence on overall climate change results. However, the variations demonstrate both positive and negative impacts on GHG emissions. For example, in Kärrbo Prästgård's fixed vertical APV system, root crops result in additional GHG emissions of 1.08 g CO_{2eq}/kWh, while forage crops provide GHG emissions savings of 1.07 g CO_{2eq}/kWh. The highest normalized GHG emissions occur with dual-axis configuration on root crops in Kärrbo Prästgård (29.1 g CO_{2eq}/kWh), while the lowest emissions are achieved with interspace single-axis configuration on berries in Agrigento (11.2 g CO_{2eq}/kWh).

National grid mixes show the largest footprints among the electricity sources considered, with 645 g CO_{2eq}/kWh for Germany, 436.6 g CO_{2eq}/kWh for Italy, and 45.4 g CO_{2eq}/kWh for Sweden. Across all locations, APV configurations outperform both grid electricity and CGMPV systems, consistent with previous research (Agostini et al., 2021; Wagner et al., 2023; Busch and Wydra, 2023; Krexner et al., 2024; Pascaris et al., 2021; Handler and Pearce, 2022).

4.4.2. *Photochemical ozone formation, and ozone depletion*

Fig. 7 shows the normalized Photochemical Ozone Formation Potential (POFP) and Ozone Depletion Potential (ODP) of various APV configurations compared to the CGMPV system and the national

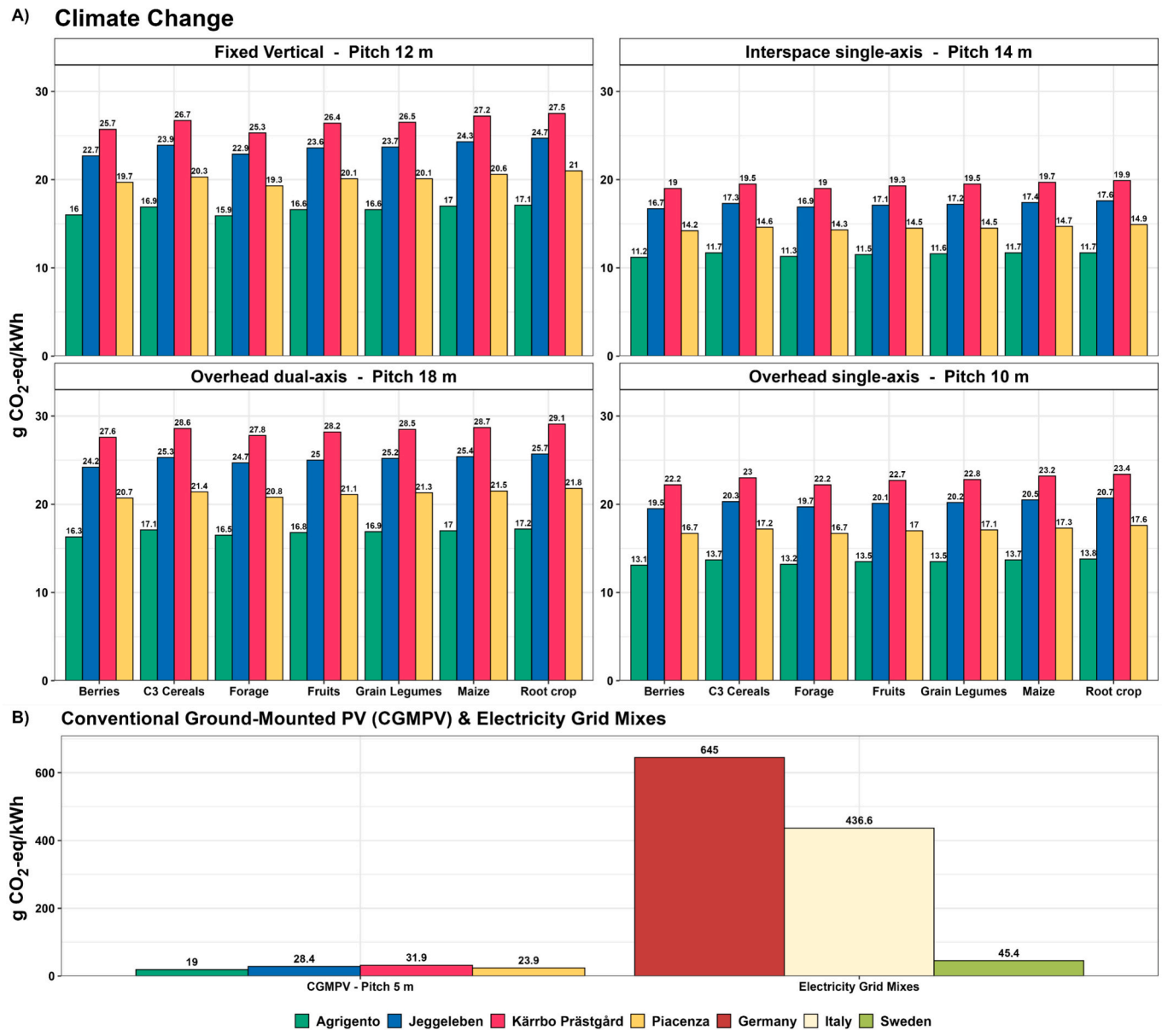

Fig. 6. Comparative GHG emissions of APVs at the medium pitch per each configuration, CGMPV, and electricity grid mixes, normalized per kWh across multiple locations and crop groups.

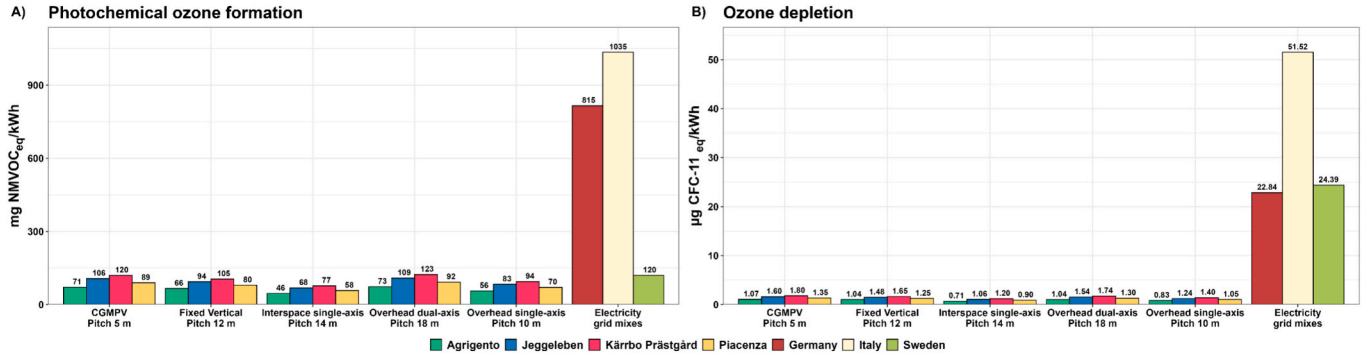

Fig. 7. Normalized photochemical ozone formation potential (A) and ozone depletion potential (B) of APV systems across different configurations and locations compared to CGMPV system and national electricity grid mix.

electricity grid mix.

For POFP (Fig. 7A), APV systems range from 46 to 123 mg NMVOC$_{eq}$/kWh. The interspace single-axis system in Agrigento (highest irradiance) demonstrates the lowest POFP (46 mg NMVOC$_{eq}$/kWh). Conversely, the overhead dual-axis APV system in Kärrbo Prästgård (lowest irradiance) exhibits the highest POFP (123 mg NMVOC$_{eq}$/kWh) due to its higher material intensity, complexity, and lower solar availability, leading to elevated normalized emissions. Most APV configurations generally outperform CGMPV systems, which average 106 mg NMVOC$_{eq}$/kWh and a peak of 120 mg NMVOC$_{eq}$/kWh in Kärrbo Prästgård. However, the worst-performing APV system in Kärrbo Prästgård slightly exceeds the peak CGMPV impact (overhead dual-axis at 123 mg NMVOC$_{eq}$/kWh). APV systems exhibit 8 to 23 times lower POFP than the Italian grid mix (1035 mg NMVOC$_{eq}$/kWh) and 7–18 times lower than the German grid mix (815 mg NMVOC$_{eq}$/kWh). While they are 1.1 to 2.6 times lower than the relatively clean Swedish grid (120 mg NMVOC$_{eq}$/kWh), the overhead dual-axis APV system in Kärrbo Prästgård (123 mg NMVOC$_{eq}$/kWh) shows a slightly higher impact than the Swedish grid. Regarding ODP (Fig. 7B), APV systems range from 714 to 1740 μg CFC-11$_{eq}$/kWh. Consistent with POFP, the interspace single-axis system in Agrigento shows the lowest ODP (714 μg CFC-11$_{eq}$/kWh), while the overhead dual-axis APV system in Kärrbo Prästgård exhibits the highest (1740 μg CFC-11$_{eq}$/kWh), primarily driven by material intensity and energy yields. All APV configurations and CGMPV systems consistently demonstrate significantly lower ODPs compared to country-level electricity grids. For instance, APV systems are 29 to 71 times lower than the Italian grid mix (51,520 μg CFC-11$_{eq}$/kWh), and 12 to 31 times lower than both the German (22,840 μg CFC-11$_{eq}$/kWh) and Swedish (24, μg CFC-11$_{eq}$/kWh) grid mixes. Notably, unlike POFP, the German grid shows a marginally lower ODP than the Swedish grid. Compared to CGMPV systems (ranging from 1070 to 1800 μg CFC-11$_{eq}$/kWh), even the worst-performing APV system (overhead dual-axis in Kärrbo Prästgård at 1740 μg CFC-11$_{eq}$/kWh) shows a slightly lower ODP than the peak CGMPV.

4.4.3. Respiratory inorganics

Fig. 8 represents the normalized respiratory inorganics (particulate matter) potential.

Within the APV configurations, impacts vary from 7.5E-10 to 2.03E-09 Disease incidence/kWh. The interspace single-axis system in Agrigento records the lowest impact (7.54E-10 Disease incidence/kWh). Conversely, the overhead dual-axis APV system in Kärrbo Prästgård shows the highest impact (2.03E-09 Disease incidence/kWh), primarily due to its greater material intensity and complexity, coupled with lower local solar availability, which inflates normalized emissions. APV systems demonstrate a significantly lower impact, ranging from 12 to 33 times less than the Italian electricity grid (approx. 2.5E-09 Disease incidence/kWh), 13–34 times less than the German grid (approx. 2.6E-08 Disease incidence/kWh), and 1.4–3.7 times less than the Swedish grid (approx. 2.78E-09 Disease incidence/kWh). The German grid shows a marginally higher impact than the Italian grid, while the Swedish grid, consistent with its generally cleaner profile, presents a significantly lower impact than both German and Italian grids in this specific category. Comparing APV to the CGMPV system, most APV systems exhibit superior performance. CGMPV impacts range from 1.31E-09 Disease incidence/kWh (Agrigento) to a peak of 2.2E-09 Disease incidence/kWh in Kärrbo Prästgård, with an average of 1.77E-09 Disease incidence/kWh. Notably, even the worst-performing APV system (overhead dual-axis in Kärrbo Prästgård at 2.03E-09 Disease incidence/kWh) shows a lower impact than the peak CGMPV system. A similar trend has been documented by (Agostini et al., 2021; Wagner et al., 2023; Busch and Wydra, 2023; Krexner et al., 2024).

4.4.4. Acidification

Fig. 9 signifies the normalized acidification potential.

Examining the APV configurations, acidification impacts range from a low of 0.1 mmol H + $_{eq}$/kWh for the interspace single-axis system in Agrigento to a high of 0.21 mmol H + $_{eq}$/kWh for the fixed vertical APV system in Kärrbo Prästgård. APV systems demonstrate impacts that are 22 to 48 times lower than the Italian grid (approx. 4.72 mmol H + $_{eq}$/kWh) and 22 to 47 times lower than the German grid (approx. 4.54 mmol H + $_{eq}$/kWh). Even against the comparatively cleaner Swedish grid (approx. 0.24 mmol H + $_{eq}$/kWh), APV systems achieve a significant reduction, showing impacts 1.1 to 2.4 times less. Notably, the Swedish grid exhibits a substantially lower acidification burden than both its Italian and German counterparts, reflecting distinct profiles of acidifying substance emissions from their respective energy generation and industrial activities. When contrasted with the CGMPV system, APV systems generally present a more favorable environmental profile. CGMPV impacts span from 0.15 mmol H + $_{eq}$/kWh (Agrigento) to a peak of 0.26

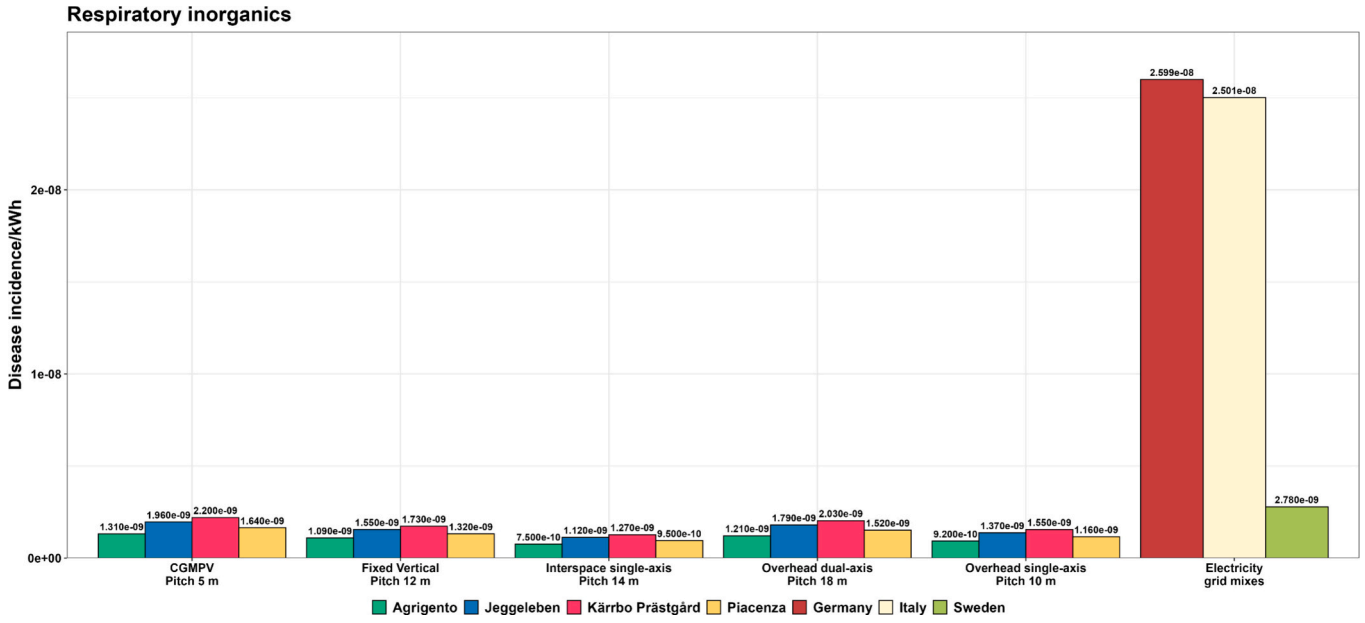

Fig. 8. Normalized respiratory inorganics potential of APV systems across different configurations and locations compared to CGMPV system and national electricity grid mix.

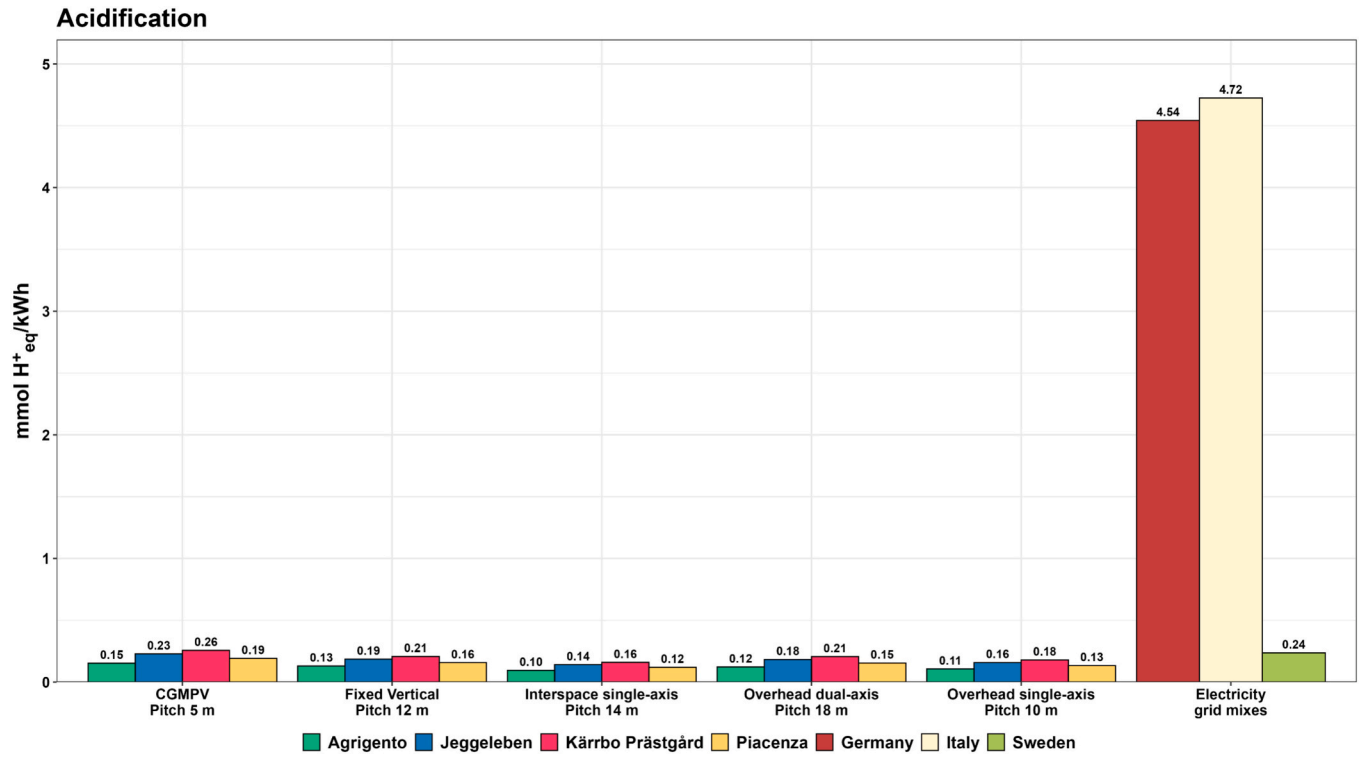

Fig. 9. Normalized acidification potential of APV systems across different configurations and locations compared to CGMPV system and national electricity grid mix.

mmol H + $_{eq}$/kWh in Kärrbo Prästgård, with an average of 0.18 mmol H + $_{eq}$/kWh. Crucially, even the highest-impact APV system records a lower impact than the peak CGMPV system and national grid mix, which are in line with (Agostini et al., 2021; Wagner et al., 2023; Busch and Wydra, 2023; Krexner et al., 2024).

4.4.5. *Eutrophication: Freshwater, terrestrial, and marine*

Fig. 10 presents the normalized eutrophication potential for freshwater eutrophication (A), terrestrial eutrophication (B), and marine eutrophication (C).

For Freshwater Eutrophication (Fig. 10A), the German grid shows the highest impact at ~916 mg P_{eq}/kWh, far exceeding the Italian (~129 mg P_{eq}/kWh) and Swedish (~21 mg P_{eq}/kWh) grids. APV systems are much lower, 12–26 mg P_{eq}/kWh, which is 34.5–73.6 times less than the German grid and 4.9–10.4 times less than the Italian grid. APV is generally comparable to or only slightly higher (≤1.3 times) than the Swedish grid. The interspace single-axis in Agrigento records the lowest impact (12 mg P_{eq}/kWh), while the overhead dual-axis in Kärrbo Prästgård is highest (26 mg P_{eq}/kWh). Compared with CGMPV (17–29 mg P_{eq}/kWh), most APV systems perform better, with the best achieving a 27 % reduction and even the highest APV below the CGMPV peak. In terms of Terrestrial Eutrophication (Fig. 10B), Germany again leads with ~17 mmol N_{eq}/kWh, followed by Italy (~15 mmol N_{eq}/kWh) and Sweden (~0.75 mmol N_{eq}/kWh). APV systems (0.15–0.36 mmol N_{eq}/kWh) are 47–111 times lower than Germany and 42–98 times lower than Italy, though up to 2.3 times higher than Sweden. The interspace single-axis in Agrigento has the lowest value (0.15 mmol N_{eq}/kWh) and the overhead dual-axis in Kärrbo Prästgård the highest (0.36 mmol N_{eq}/kWh). Most APVs outperform CGMPV (0.26–0.43 mmol N_{eq}/kWh), with the most efficient APV showing a 40 % reduction and the highest APV still below the CGMPV peak. For Marine Eutrophication (Fig. 10C), the German grid reaches ~555 mg N_{eq}/kWh, followed by Italy (~417 mg N_{eq}/kWh) and Sweden (~60 mg N_{eq}/kWh). APV systems (14–33 mg N_{eq}/kWh) are 16–39 times lower than Germany and 12–29 times lower than Italy, and up to 4.2 times lower than Sweden. The interspace single-axis in Agrigento records the lowest impact (14 mg N_{eq}/kWh), while the overhead dual-axis in Kärrbo Prästgård records the highest (33 mg N_{eq}/kWh). Compared with CGMPV (23–38 mg N_{eq}/kWh), APV generally performs better, with the most efficient APV reducing impacts by 27 % and the highest APV still below the CGMPV peak. All eutrophication results align with prior studies (Agostini et al., 2021; Wagner et al., 2023; Busch and Wydra, 2023; Krexner et al., 2024).

4.4.6. *Resource use*

Fig. 11 presents the normalized resource use for fossil (energy carriers), and for minerals and metals.

A pronounced disparity in "Resource use, fossils (Fig. 11B)" is evident between country-level electricity grids and solar PV technologies. Grids exhibit significantly higher impacts due to reliance on fossil fuels, directly depleting non-renewable energy carriers. The German grid records the highest impact at approximately 8.88 MJ/kWh, followed by the Italian and Swedish grids at around 6.38 and 5.93 MJ/kWh. In contrast, APV systems range from 0.14 to 0.33 MJ/kWh, equal to 18–64 times less than the respective grids. CGMPV spans 0.22–0.37 MJ/kWh, and the most efficient APV configuration achieves a 37 % reduction versus the lowest CGMPV, while even the highest-impact APV remains below the peak CGMPV. This trend is consistent with (Agostini et al., 2021; Wagner et al., 2023; Busch and Wydra, 2023; Krexner et al., 2024; Pascaris et al., 2021).

Regarding "resource use, mineral and metals" category (Fig. 11A), a distinct trend emerges relative to other categories. National grids show lower impacts, with Sweden at approximately 0.16 mg Sb_{eq}/kWh, Italy at around 0.18 mg Sb_{eq}/kWh, and Germany at approximately 0.21 mg Sb_{eq}/kWh. APV systems range from 0.75 to 1.52 mg Sb_{eq}/kWh, which is 3.5–7.2 times higher than Germany's grid, 4.1–8.3 times higher than Italy's, and 4.7–9.6 times higher than Sweden's. Within APV, the fixed vertical system in Kärrbo Prästgård is highest at 1.52 mg Sb_{eq}/kWh, largely due to ~12 % higher steel intensity and lower solar availability inflating normalized results, while the interspace single-axis in Agrigento is lowest at 0.75 mg Sb_{eq}/kWh. CGMPV ranges from 0.77 to 1.30 mg Sb_{eq}/kWh; the most efficient APV is only marginally above the lowest CGMPV, whereas the highest-impact APV can exceed the peak

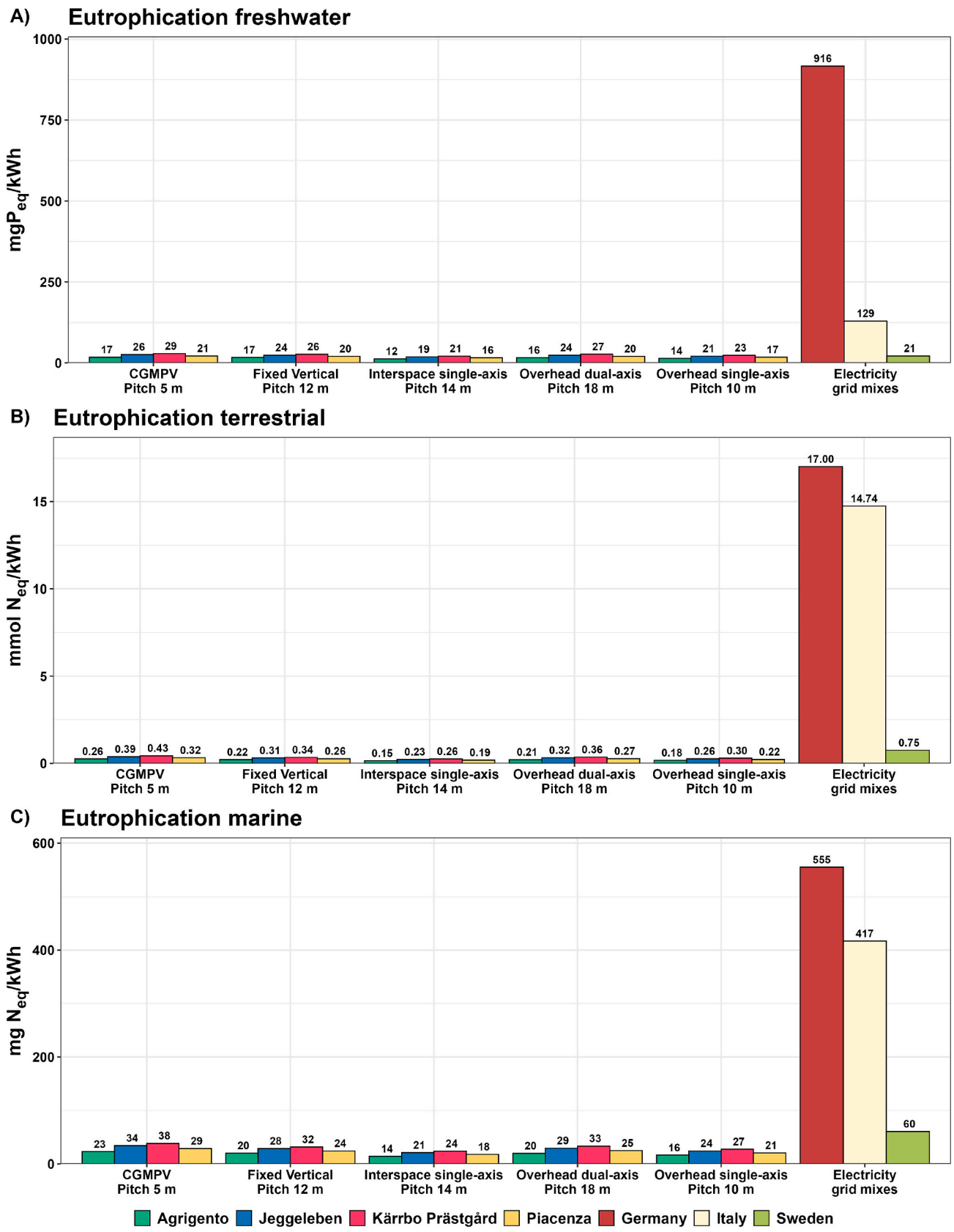

Fig. 10. Normalized eutrophication potentials for freshwater (A), terrestrial (B), and marine (C) across various APV configurations compared to the CGMPV system and the national electricity grid mix.

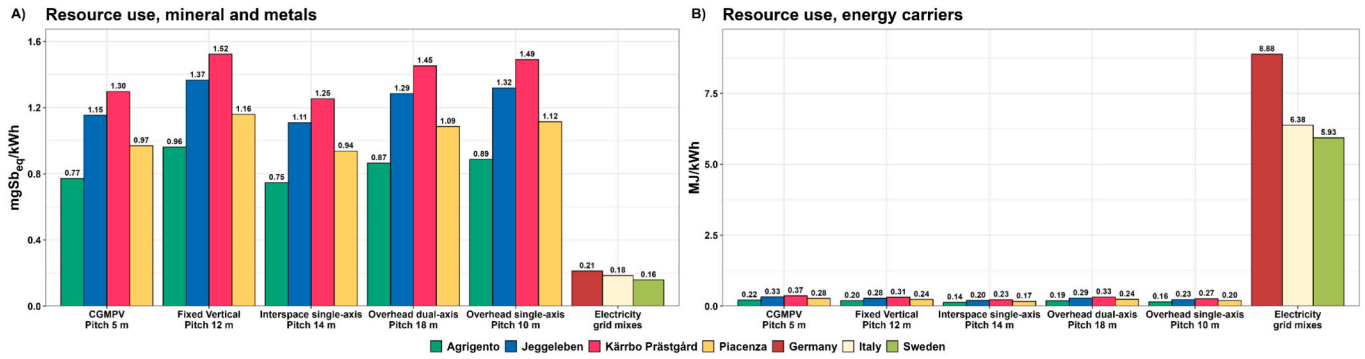

Fig. 11. Normalized resource use potentials- minerals and metals (A) and fossils (B)-for various APV systems and locations, compared to the CGMPV system and national electricity grid mix.

CGMPV. These findings align with (Agostini et al., 2021; Wagner et al., 2023; Busch and Wydra, 2023; Krexner et al., 2024).

4.5. Uncertainty analysis

To assess the robustness of the results, a Monte Carlo Analysis was performed using SimaPro. The analysis focused solely on the PV component materials, as their contribution exceeded 95 % of the total GHG emissions across all configurations, whereas the consequential elements accounted for less than 5 % (see Sections 3.1–3.3). Due to this imbalance, the uncertainty analysis was restricted to the attributional portion of the LCA.

Among the ten impact categories evaluated, Climate Change and Resource Use (Minerals and Metals) were selected for uncertainty analysis, as these categories showed the highest sensitivity in distinguishing between different APV configurations and the CGMPV system (see Section 3.4). The remaining categories exhibited minimal variability, with impact values clustering tightly (detailed results are available in Fig. S4 in SI1).

Country-level electricity grid mixes were excluded from this analysis as their absolute impact values were orders of magnitude higher than those of APV and CGMPV systems. Furthermore, SimaPro defines grid inventories per unit of energy produced, making it incompatible with fixed-capacity comparisons like the 1 MW_p system size used here.

To improve visual interpretability, the probability distributions were smoothed using a moving average with a window size of three. Fig. 12 presents the resulting distributions for the selected categories across all APV configurations and the CGMPV system, normalized to 1 MW_p installed capacity.

In the climate change category (left), the fixed vertical and interspace single-axis systems exhibit very similar distributions, both displaying narrow peaks concentrated at lower CO_{2eq} values. This suggests a consistently low climate impact across simulations for these two APV configurations. Their probability distributions are skewed, with most values falling between approximately 600 and 850 t CO_{2eq}, indicating that they are likely to result in lower emissions compared to the other systems analyzed. Interestingly, the overhead single-axis system performs better than might be expected for an elevated structure. Its distribution is generally lower than that of the CGMPV, with most values concentrated below 850 t CO_{2eq}. Although its climate impact is slightly higher than the fixed vertical and interspace single-axis configurations, it remains relatively modest. This indicates that the elevated mounting structure does not necessarily translate to significantly higher emissions, especially when compared to CGMPV systems. Notably, despite being structurally more demanding than its interspace counterpart, the overhead single-axis system exhibits lower average climate impacts than CGMPV, potentially due to more efficient use of materials such as steel and foundation elements.

The CGMPV system shows a broader distribution centered around 900 t CO_{2eq}, suggesting greater variability and a tendency toward higher emissions. It typically results in more substantial climate impacts than the fixed vertical, interspace single-axis, and overhead single-axis

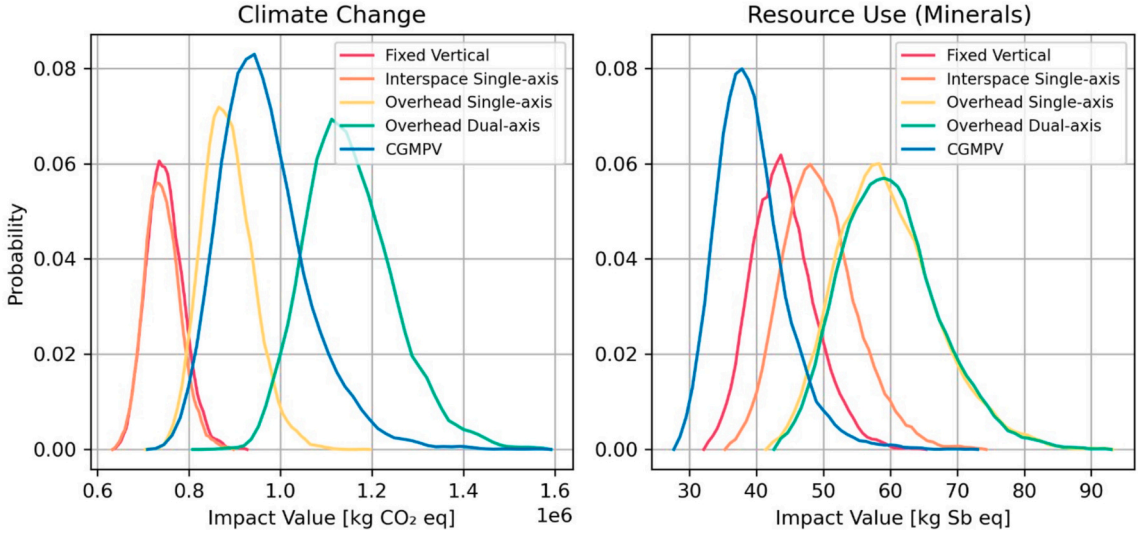

Fig. 12. Smoothed probability distributions of life cycle impact values for APV configurations and CGMPV system (Monte Carlo uncertainty analysis for Climate Change and Resource Use impact categories, normalized to 1 MW_p system capacity, PV components only).

systems. Nonetheless, its distribution does overlap with those of other configurations, reflecting that in specific contexts or design implementations, CGMPV can still achieve relatively low emissions. In contrast, the overhead dual-axis system exhibits the highest climate change impacts overall, with a distribution that is both wide and right-skewed, extending up to approximately 1600 t CO_{2eq}. This indicates a combination of high average emissions, likely driven by the increased structural and mechanical complexity required for dual-axis tracking and elevated module mounting. However, it is important to note that, despite the generally higher impacts associated with overhead dual-axis systems, the sensitivity analysis occasionally reveals lower emissions compared to CGMPV or overhead single-axis configurations. Such outcomes are consistent with scenarios in which competing systems underestimate their material requirements or where dual-axis designs achieve reduced material needs. The right panel shows the results for mineral resource use, where CGMPV demonstrates the lowest impact across all systems. Its sharply peaked distribution, centered around 38 kg Sb_{eq}, reflects low and consistent material demands. The fixed vertical system also performs well, with its distribution confined mainly to the 32–60 kg Sb_{eq} range. This suggests modest material requirements, likely due to its ground-mounted, structurally simple design. The interspace single-axis configuration displays a somewhat broader distribution that overlaps with the fixed vertical system but also extends toward higher impact values. While it can match the resource efficiency of simpler systems in some cases, it also shows a higher probability of increased mineral use, possibly due to additional tracking mechanisms or structural reinforcement. The overhead single-axis and overhead dual-axis systems show nearly identical and significantly wider distributions, peaking around 60 kg Sb_{eq} and extending beyond 90 kg Sb_{eq}. These results reflect the substantial material requirements for elevated, mechanically tracked systems. The similarity between these two configurations suggests that the elevated structure itself, rather than the number of tracking axes, is the dominant contributor to mineral resource intensity. While overhead systems are clearly more resource-intensive (Agostini et al., 2021), they offer key functional advantages such as increased clearance for machinery access, and crop operations (Bellone et al., 2024). These design benefits may be crucial in certain APV applications despite the environmental trade-offs.

5. Discussion

5.1. APV structural land occupation

The nearly twofold variation in land occupation across designs therefore translates directly into a similar variation in environmental impact. The poor performance of the overhead single-axis system is not just a matter of occupying more space; its extensive land exclusion is the direct cause of it generating the highest GHG emissions (19.12 t CO_{2eq}). Conversely, the superior land-use efficiency of the overhead dual-axis system, achieved through its optimized design of moderate module density and short structural lengths (REM TEC S.R.L., 2025), allows it to produce the lowest emissions (9.35 t CO_{2eq}). Interestingly, while the interspace single-axis system has a much longer structural length (Valmont Solar, 2025), its exceptionally high module density reduces the number of trackers needed (Table 5), leading to slightly better land-use efficiency. These findings highlight that structural design is a key factor in balancing energy conversion with agricultural land preservation while also determining ILUC-related GHG emissions and their resulting climate impacts.

5.2. Crop yield variations

The higher GHG emissions observed for most crops under the overhead dual-axis system are attributable to its greater shading intensity relative to single-axis configurations, consistent with previous studies linking APVs design choices to higher climate impacts (Sponagel et al., 2024). A noteworthy observation emerges when comparing the two single-axis configurations. Although the interspace single-axis system has higher shading levels, it consistently shows lower total GHG emissions from yield loss than the overhead single-axis system. This occurs because the interspace system has a substantially smaller net cultivable land area available per megawatt, approximately 50 % less (Table 7), which reduces the total crop loss and the resulting ILUC-related GHG emissions (Agostini et al., 2021; Sponagel et al., 2024; Bellone et al., 2024).

5.3. PV components

GHG emissions from PV components underscore the importance of structural optimization for the environmental performance of APVs. Steel was the dominant contributor, accounting for 118.6 t CO_{2eq} in the interspace system and up to 520.7 t CO_{2eq} in the dual-axis system. This finding confirms that structural BOS components are key environmental hotspots, as consistently reported in previous studies (Agostini et al., 2021; Sponagel et al., 2024). The substantial variation, up to 55 % between the most and least material-intensive configurations, can be attributed almost entirely to the amount of steel required for mounting structures, which is largely determined by design parameters such as installation height. These results clearly demonstrate that structural design choices have a decisive influence on the overall climate impact of APV installations.

5.4. Climate change

Across APV configurations, the climate change hierarchy is governed by structural height and associated steel demand, together with the added complexity of dual-axis actuation, which raises GHG impacts relative to single-axis alternatives, consistent with previous studies (Agostini et al., 2021). Systems with lower installation heights, such as the interspace single-axis design, require less steel and therefore achieve the lowest embodied emissions across sites. By contrast, the overhead dual-axis configuration has the highest impacts because taller supports and more complex mechanisms substantially increase material needs. Normalizing by electricity generation reduces but does not eliminate differences. Higher-yield trackers spread embodied burdens over more kWh, which is why the overhead single-axis system outperforms the fixed vertical configuration despite additional components. The geographic gradient from Agrigento to Kärrbo Prästgård reflects the primacy of solar resource, as higher irradiation in southern Europe lowers carbon intensity per kWh. Land occupation and crop-specific yield effects become minor once normalized, with crop responses to shading remaining secondary to structural material intensity and energy yield. Grid footprints mirror generation mixes (Fig. S3 in SI1). Sweden's grid is predominantly low-carbon, with nuclear 42.2 % and hydropower 41.6 %. As shown in Fig. S3 (SI1), Italy is led by natural gas at 33.5 %, with hydropower 21.5 % and coal 16.6 %. Germany is the most fossil-intensive, dominated by coal at 45.4 %, with nuclear 15.5 % and natural gas 9.9 %. These structural differences in electricity generation technologies, particularly Germany's heavy reliance on coal, directly explain the pronounced variation in GHG emissions across the countries. Benchmarked against CGMPV and national grids, all APV systems show lower GHG intensities, in line with (Agostini et al., 2021; Wagner et al., 2023; Busch and Wydra, 2023; Krexner et al., 2024; Pascaris et al., 2021; Handler and Pearce, 2022). The advantage is greatest where coal dominates, as in Germany, yet remains evident even against Sweden's low-carbon mix. Overall, the results underscore the decarbonization potential of APV and confirm that minimizing steel while maintaining high energy yield is critical to achieving the lowest climate impacts.

5.5. Photochemical ozone formation, and ozone depletion

The analysis of APV systems highlights their performance for both

POFP and ODP, showing strong dependence on system design, material intensity, and solar irradiance. The interspace single-axis system performs best due to its optimized balance of material inputs and energy yield, achieving a 57 % reduction in ozone precursor emissions compared with the average CGMPV. This also illustrates that not all APV configurations consistently outperform CGMPV, particularly in low-irradiance settings where the advantage narrows. Significant environmental gains arise when APV displaces grid electricity. Both impact categories underscore the importance of renewable deployment for reducing tropospheric ozone precursors and protecting the stratospheric ozone layer, particularly when substituting fossil fuel-intensive electricity. Interestingly, in contrast to POFP, the German grid exhibits a slightly lower ODP than the Swedish grid. This finding is counter-intuitive, given that Germany's electricity generation is largely coal-based (45.38 %), whereas Sweden relies predominantly on low-carbon sources (see Fig. S3 in SI1). However, this outcome reflects the specific life-cycle inventory data in the Ecoinvent v3.8 database, which attribute higher ODP to the upstream supply chains of nuclear and hydropower technologies in Sweden. Overall, APVs generally perform comparably to or better than CGMPV for ozone depletion, even under less favorable conditions, consistent with previous findings (Agostini et al., 2021; Wagner et al., 2023; Busch and Wydra, 2023).

5.6. Respiratory inorganics

Respiratory-inorganics impacts are driven by combustion emissions and their precursors, so cross-country differences closely follow generation portfolios. Germany's coal-intensive grid mix (Fig. S3 in SI1) produces the highest disease-incidence burden, Italy shows intermediate impacts due to its natural-gas dominance with residual coal, and Sweden is much lower because nuclear and hydropower supply most of its generation. Against these baselines, all APV configurations are far lower. Within APV, performance reflects structural material intensity and solar resource. The interspace single-axis configuration achieves the lowest impacts in high-irradiance locations, where optimized structures and higher yields dilute manufacturing-phase particulate emissions per kWh. The overhead dual-axis configuration shows the highest impacts in low-irradiance northern sites, where greater mechanical complexity and lower generation raise normalized burdens. APV systems generally outperform CGMPV at the same sites, showing that yield gains from tracking and lean BOS inventories offset the simpler ground-mounted baseline, consistent with previous studies (Agostini et al., 2021; Wagner et al., 2023; Busch and Wydra, 2023; Krexner et al., 2024). Overall, replacing combustion-based electricity with APV provides substantial public-health benefits, with the greatest marginal gains in coal-heavy grids. Prioritizing configurations that minimize structural material while maximizing generation further reduces respiratory-inorganics impacts and strengthens APVs' role in mitigating adverse respiratory health outcomes.

5.7. Acidification

Acidification impacts are mainly driven by sulfur and nitrogen oxides from combustion. Germany's coal-heavy mix substantially elevates sulfur dioxide (SO_2) and nitrogen oxides (NO_x) emissions, creating the largest gap between its grid mix and APV systems. Italy's natural-gas-dominated mix lowers SO_2 but retains significant NO_x and a coal share, yielding intermediate impacts. Sweden's reliance on nuclear and hydropower suppresses combustion-related precursors and narrows the margin to APV, though APV still retains a clear advantage. Within APVs, impacts depend on structural material intensity and solar resource. Lean, high-yield designs, such as the interspace single-axis system in Agrigento, dilute manufacturing emissions per kWh, whereas heavier structures in low-irradiance sites, such as the fixed vertical system in Kärrbo Prästgård, raise normalized burdens. Overall, the most efficient APV achieves a 48 % reduction in acidification impacts compared with the average CGMPV, confirming APV's consistent environmental advantage across conditions and supporting previous findings (Agostini et al., 2021; Wagner et al., 2023; Busch and Wydra, 2023; Krexner et al., 2024).

5.8. Eutrophication: Freshwater, terrestrial, and marine

Germany's coal-heavy mix releases the most phosphorus- and nitrogen-bearing precursors, explaining the large gap to PV. Italy's natural-gas-led mix yields intermediate burdens, while Sweden's nuclear and hydropower dominance suppresses combustion precursors and results in much lower values, especially for terrestrial and marine outcomes. These differences explain APVs' 34.5–73.6 times advantage over Germany, 4.9–10.4 times over Italy in freshwater eutrophication, and similarly wide margins in the other subcategories. Within PV, differences are driven by structural mass and solar resource. Material-efficient, high-yield designs such as the interspace single-axis in Agrigento dilute manufacturing emissions, while heavier structures in low-irradiance sites, such as the overhead dual-axis or fixed vertical in Kärrbo Prästgård, raise normalized burdens but remain below CGMPV and far below grid levels. Overall, displacing combustion-based electricity with APV greatly reduces eutrophication across freshwater, terrestrial, and marine environments. The largest gains occur in coal-heavy grids, and within APVs the most effective strategy is combining lean support structures with high-irradiation sites to minimize impacts.

5.9. Resource use

For fossil resource use, the grid ranking reflects fuel portfolios. Germany's coal-heavy mix, Italy's substantial natural-gas share with residual coal, and Sweden's comparatively lower-fossil mix explain the order and the wide margins to PV. Solar PV avoids fuel combustion during operation; residual burdens stem from material supply chains and are diluted at high-irradiance sites, which is why APV options fall 18–64 times below the grids and frequently below CGMPV.

For mineral and metal resource use, the pattern reverses because the category tracks primary extraction of metals and minerals. Grid electricity relies largely on existing centralized assets with modest incremental material flows per kWh, whereas PV is fabrication-intensive. APVs increase structural demand relative to CGMPV, and designs with taller supports or greater steel content, coupled with low irradiance, raise normalized burdens. Thus the fixed vertical system in Kärrbo Prästgård sits at the upper end, while the interspace single-axis in Agrigento benefits from a material-efficient structure and strong yield. These trends in both subcategories of "Resource Use" are consistent with previous findings (Agostini et al., 2021; Wagner et al., 2023; Busch and Wydra, 2023; Krexner et al., 2024; Pascaris et al., 2021).

These contrasts point to actionable levers. For fossil resource use, any displacement of combustion-based electricity generation by APV confers immediate gains, with the largest benefits in fossil-intensive grids. For mineral and metal use, optimizing structural mass and layout, prioritizing high-irradiance siting, and advancing circularity and recycled content can materially reduce impacts. Overall, APV retains a clear advantage for non-renewable fossil resource depletion while requiring careful structural and supply-chain choices to manage mineral and metal use.

5.10. Study limitations and future directions

This comprehensive LCA study reveals clear environmental performance hierarchies while operating within methodological boundaries that inform future research priorities. The cradle-to-end-of-use system boundary necessarily excludes EOL phase impacts due to insufficient reliable data for component recycling and disposal pathways. This limitation, though applied consistently across all configurations to maintain comparability, prevents full assessment of circular economy

potential for systems containing substantial steel infrastructure ranging from 53.8 to 236.2 tons per megawatt peak.

Material inventories obtained directly from commercial manufacturers represent real-world deployed systems rather than theoretical designs, yet this specificity may limit generalizability across the broader technology landscape. While Monte Carlo Analysis confirmed that performance rankings remain statistically robust despite input variability, absolute impact values may differ across manufacturers due to proprietary designs and structural variations. This uncertainty becomes particularly relevant given that steel consumption emerged as the dominant differentiating factor among configurations, suggesting that future research investigating alternative materials could substantially reduce both climate impacts and mineral resource depletion.

The assessment of agricultural impacts relies on meta-analytical regression models calibrated from existing APV studies rather than site-specific field measurements, introducing uncertainty in crop yield predictions across diverse pedoclimatic conditions. Similarly, ILUC emissions employ a static factor consistent with EU guidelines, which simplifies complex regional agricultural dynamics. However, these contributions proved relatively minor, accounting for less than 5 % of total GHG emissions, suggesting that refinements to these factors would not substantially alter the comparative results.

The analysis utilizes Ecoinvent v3.8 integrated within SimaPro v9, which, while scientifically robust and widely cited, may not reflect the most recent refinements to background data, particularly for national electricity grid mixes found in newer database versions. Additionally, the temporal dimension of both electricity generation and climate conditions presents opportunities for enhanced analysis. Historical climate data spanning 2000 to 2024 captures substantial interannual variability including extreme events, yet assumes stationarity that may not adequately represent future conditions for infrastructure with thirty-year operational lifespans. Furthermore, the analysis based on annual average electricity production overlooks the potential value of tracking and vertical systems energy conversion during morning and afternoon peaks when they may displace carbon-intensive fossil fuel generation.

Future investigations should prioritize comprehensive cradle-to-grave assessments as recycling technologies mature and EOL data becomes available. Long-term field trials across diverse agricultural systems would strengthen crop yield models while accounting for emerging shade-tolerant cultivars and management adaptations specific to APV environments. Integration of climate change projections would assess system resilience under non-stationary conditions, while Social Life Cycle Assessment (S-LCA) would capture broader sustainability dimensions including rural employment, energy justice, and community acceptance factors that influence successful deployment. These research directions would collectively strengthen the evidence base for optimizing APV systems within sustainable food-energy transitions.

6. Conclusion

This study conducted a comprehensive LCA to quantify the environmental performance of four APV configurations across different European climates, providing critical insights for sustainable energy and agricultural planning. The results clearly demonstrate that the choice of APV design is a paramount factor influencing its overall environmental footprint.

The principal finding is the superior performance of the interspace single-axis APV system, which consistently yielded the lowest environmental impacts across nearly all ten investigated categories. For instance, its GWP ranged from approximately 11 to 20 g CO_{2eq}/kWh. In stark contrast, the overhead dual-axis system was the least environmentally favorable, with a GWP of 16 to 29 g CO_{2eq}/kWh.

In stark contrast, the overhead dual-axis system, despite its advanced tracking capabilities, it was still the least environmentally favorable configuration due to its significant material intensity, particularly due to the large quantity of steel required for its elevated structure. The fixed vertical and overhead single-axis systems showed intermediate performance, highlighting a clear trade-off between structural complexity, material demand, and energy conversion efficiency. The impacts from the consequential approach, accounting for crop yield variations and structural land occupation, contributed less than 5 % to the total GHG emissions, making them secondary to the component-related impacts.

When benchmarked against conventional energy systems, all APV configurations offered dramatic improvements over electricity grid mixes in nine out of ten impact categories, underscoring their potential to drive deep decarbonization and mitigate issues like acidification, eutrophication, and air pollution. Furthermore, most APV designs outperformed CGMPV in environmental impacts, especially in climate change. This indicates that land dual-use does not inherently increase environmental burdens per unit of energy. Interspace single-axis, fixed vertical, and overhead single-axis APVs performed better overall, while the overhead dual-axis system, despite some benefits, underperformed CGMPV in certain high-impact cases, such as photochemical ozone formation in low-irradiance areas, due to its higher material intensity. The one exception was mineral and metal resource use, where all PV systems were more impactful than grid electricity, highlighting the material intensity of PV infrastructure. Crucially, the Monte Carlo Analysis confirmed the robustness of these findings. It showed that the performance rankings are statistically significant, with clear distinctions between the system configurations despite variability in background data. This gives strong confidence that the observed differences are inherent to the system designs rather than being artifacts of data uncertainty. While overhead systems provide greater clearance for agricultural machinery, this functionality comes at a considerable environmental cost. Our findings advocate for the preferential deployment of material-efficient like the interspace single-axis system where agricultural practices permit.

Nomenclature

APV	Agrivoltaic
BOS	Balance of System
CDF	Cumulative Distribution Function
CGMPV	Conventional Ground-Mounted Photovoltaic
CFC-11	Trichlorofluoromethane
CO_2	Carbon Dioxide
CO_{2eq}	Carbon Dioxide Equivalent
CY	Crop Yield
EF	Environmental Footprint
EOL	End-of-Life
ERA5	European Centre for Medium-Range Weather Forecasts Reanalysis
FL	Full Light
FS	Finkelstein–Schafer
FU	Functional Unit
GHG	Greenhouse Gas
GHI	Global Horizontal Irradiance
GWP100	Global Warming Potential (100 years)
ha	Hectare
HF	Hydrogen Fluoride
HNO_3	Nitric Acid
HCl	Hydrochloric Acid
H_2SO_4	Sulfuric Acid
H_2O_2	Hydrogen Peroxide
Hz	Hertz
IEA	International Energy Agency
ILCD	International Life Cycle Data System
ILUC	Indirect Land Use Change
ISO	International Organization for Standardization
KOH	Potassium Hydroxide
kWh	Kilowatt-hour
LC-CO_2	Life Cycle Carbon Dioxide

LCA	Life Cycle Assessment
LCI	Life Cycle Inventory
LCIA	Life Cycle Impact Assessment
MJ	Megajoule
MLR	Multiple Linear Regression
Mt. CO_{2eq}	Million metric tons of Carbon Dioxide Equivalent
MWp	Megawatt peak
N_2	Nitrogen
NH_3	Ammonia
NMVOC	Non-Methane Volatile Organic Compounds
NREL	National Renewable Energy Laboratory
O_2	Oxygen
ODP	Ozone Depletion Potential
PAR	Photosynthetically Active Radiation
PET	Potential Evapotranspiration
$POCl_3$	Phosphorus Oxychloride
POE	Polyolyaltha Olefin
PV	Photovoltaic
RH	Relative Humidity
RoW	Rest of the World
Sb	Antimony
Si	Silicon
SPEI	Standardized Precipitation Evapotranspiration Index
T_a	Air Temperature
TMY	Typical Meteorological Year

CRediT authorship contribution statement

Amirhossein Nik Zad: Writing – review & editing, Writing – original draft, Visualization, Validation, Software, Methodology, Investigation, Formal analysis, Data curation, Conceptualization. **Alessandro Agostini:** Writing – review & editing, Methodology, Investigation, Formal analysis, Conceptualization. **Giorgio Impollonia:** Writing – review & editing, Visualization, Formal analysis. **Sebastian Zainali:** Writing – review & editing, Writing – original draft, Visualization. **Michele Croci:** Writing – review & editing. **Michele Colauzzi:** Writing – review & editing. **Pietro Elia Campana:** Writing – review & editing, Writing – original draft. **Stefano Amaducci:** Writing – review & editing, Supervision, Methodology, Investigation, Funding acquisition, Formal analysis, Data curation, Conceptualization.

Declaration of Generative AI and AI-assisted technologies in the writing process

During the preparation of this work the authors used ChatGPT (Open-AI) to assist in refining the language and improving the readability of the manuscript. After using this tool/service, the authors thoroughly reviewed and edited the content as needed and take(s) full responsibility for the content of the publication.

Declaration of competing interest

The authors declare the following financial interests/personal relationships which may be considered as potential competing interests: The company European Energy is financing half of Sebastian Zainali's Ph.D. salary.

Acknowledgements

Amirhossein Nik Zad was supported by the PhD in Agro-Food System (Agrisystem) and by Portus project funded by Romeo and Enrica Invernizzi Foundation. Michele Croci was partially supported by "National Research Centre for Agricultural Technologies (Agritech)" CN00000022.PNRR-M4C2, Investment 1.4—Funded by the European Union— NextGenerationEU'—CUP: J33C22001160007. Financial support was also received from the Swedish Energy Agency through the project "The Solar Electricity Research Centre (SOLVE)", grant number 52693–1, and the project "MATRIX", grant number P2022-00809. Special thanks are extended to the industry partners who contributed detailed material inventory data for the LCA analysis. REM TEC® provided data for the dual-axis APV system specifications, Valmont Solar® for the single-axis APV systems data, and SentNet® for the vertical APV system information.

Appendix A. Supplementary data

Supplementary data to this article can be found online at https://doi.org/10.1016/j.spc.2025.10.003.

Data availability

Data will be made available on request.

References

Agostini, A., Battini, F., Giuntoli, J., Tabaglio, V., Padella, M., Baxter, D., Marelli, L., Amaducci, S., 2015. Environmentally sustainable biogas? The key role of manure co-digestion with energy crops. Energies 8 (6), 5234–5265.
Agostini, A., Colauzzi, M., Amaducci, S., 2021. Innovative agrivoltaic systems to produce sustainable energy: an economic and environmental assessment. Appl. Energy 281, 116102.
Amaducci, S., Yin, X., Colauzzi, M., 2018. Agrivoltaic systems to optimise land use for electric energy production. Appl. Energy 220, 545–561.
Arthur, P., Drahi, E., Badosa, J., Blanc, P., 2024. Comprehensive methodology applied to solar radiation prediction for dual use for vertical agrivoltaics system. In: EUPVSEC: 41st European Photovoltaic Solar Energy Conference, p. 8. , September.
Beguería, S., Vicente-Serrano, S.M., Reig, F., Latorre, B., 2014. Standardized precipitation evapotranspiration index (SPEI) revisited: parameter fitting, evapotranspiration models, tools, datasets and drought monitoring. Int. J. Climatol. 34 (10), 3001–3023.
Bellone, Y., Croci, M., Impollonia, G., Zad, A.N., Colauzzi, M., Campana, P.E., Amaducci, S., 2024. Simulation-based decision support for Agrivoltaic systems. Appl. Energy 369, 123490.
Busch, C., Wydra, K., 2023. Life cycle assessment of an agrivoltaic system with conventional potato production. Journal of Renewable and Sustainable Energy 15 (4).
Chavez, D.L., Azzaro-Pantel, C., Montignac, F., Ruby, A., 2025. Integrating life cycle assessment in multi-objective optimization of green hydrogen systems: a review of literature and methodological challenges. Renew. Sust. Energ. Rev. 217, 115689.
Cheng, H., Zhou, X., Yang, Y., Xu, L., Ding, Y., Yan, T., Li, Q., 2024. Environmental damages, cumulative exergy demand, and economic assessment of Panus giganteus farming with the application of solar technology. Sci. Total Environ. 907, 168020.
Dinesh, H., Pearce, J.M., 2016a. The potential of agrivoltaic systems. Renew. Sust. Energ. Rev. 54, 299–308.
Dinesh, H., Pearce, J.M., 2016b. The potential of agrivoltaic systems. Renew. Sust. Energ. Rev. 54, 299–308.
Dupraz, C., 2023. Assessment of the ground coverage ratio of agrivoltaic systems as a proxy for potential crop productivity. Agrofor. Syst. 1–18.
Ecoinvent, 2021. Ecoinvent v3.8. Available at: https://ecoinvent.org/the-ecoinvent-database/data-releases/ecoinvent-3-8/. (Accessed 30 July 2025).
Fazio, S., Castellani, V., Sala, S., Schau, E., Secchi, M., Zampori, L., Diaconu, E., 2018. Supporting information to the characterisation factors of recommended EF Life Cycle Impact Assessment methods: new methods and differences with ILCD. https://doi.org/10.2760/090552, JRC114822.
Global economic model. GTAP. Available at https://www.gtap.agecon.purdue.edu/models/landuse.asp. Accessed: 30 July 2025.
Global land use model. GLOBIOM. Available at https://iiasa.ac.at/models-tools-data/globiom. Accessed: 30 July 2025.
Handler, R., Pearce, J.M., 2022. Greener sheep: life cycle analysis of integrated sheep agrivoltaic systems. Cleaner Energy Systems 3, 100036.
Hersbach, H., Bell, B., Berrisford, P., Hirahara, S., Horányi, A., Muñoz-Sabater, J., Nicolas, J., Peubey, C., Radu, R., Schepers, D., Simmons, A., 2020. The ERA5 global reanalysis. Q. J. R. Meteorol. Soc. 146 (730), 1999–2049.
Huawei Technologies Co., Ltd., 2025. Solar components producer. Available at: https://support.huawei.com/enterprise/en/doc/EDOC1100083285/eb33de84/technical-data/ (Accessed: 30 July 2025).
Jia, X., Zhou, C., Tang, Y., Wang, W., 2021. Life cycle assessment on PERC solar modules. Sol. Energy Mater. Sol. Cells 227, 111112.
Johansson, J., 2023. Albedo Effect in APV (Agrivoltaics): Finding and Implementing an Albedo Model for the APV Site in Kärrbo.
Kiehbadroudinezhad, M., Hosseinzadeh-Bandbafha, H., Tajuddin, S.A.F.S.A., Tabatabaei, M., Aghbashlo, M., 2025. A critical review of life cycle assessment of renewable agricultural systems. Sustain Energy Technol Assess 73, 104100.
Kim, S., Zirkelbach, D., Künzel, H.M., Lee, J.H., Choi, J., 2017. Development of test reference year using ISO 15927-4 and the influence of climatic parameters on building energy performance. Build. Environ. 114, 374–386.

Krexner, T., Bauer, A., Gronauer, A., Mikovits, C., Schmidt, J., Kral, I., 2024. Environmental life cycle assessment of a stilted and vertical bifacial crop-based agrivoltaic multi land-use system and comparison with a mono land-use of agricultural land. Renew. Sust. Energ. Rev. 196, 114321.

Kumar, N.M., Chopra, S.S., 2023. Integrated techno-economic and life cycle assessment of shared circular business model based blockchain-enabled dynamic grapevoltaic farm for major grape growing states in India. Renew. Energy 209, 365–381.

Leon, A., Ishihara, K.N., 2018a. Influence of allocation methods on the LC-CO_2 emission of an agrivoltaic system. Resour. Conserv. Recycl. 138, 110–117.

Leon, A., Ishihara, K.N., 2018b. Assessment of new functional units for agrivoltaic systems. J. Environ. Manag. 226, 493–498.

Marrou, H., Guilioni, L., Dufour, L., Dupraz, C., Wery, J., 2013. Microclimate under agrivoltaic systems: is crop growth rate affected in the partial shade of solar panels? Agric. For. Meteorol. 177, 117–132.

Mason, J.E., Fthenakis, V.M., Hansen, T., Kim, H.C., 2006. Energy payback and life-cycle CO2 emissions of the BOS in an optimized 3.5 MW PV installation. Prog. Photovolt. Res. Appl. 14 (2), 179–190.

Méndez, L., Forniés, E., Garrain, D., Vázquez, A.P., Souto, A., Vlasenko, T., 2021. Upgraded metallurgical grade silicon and polysilicon for solar electricity production: a comparative life cycle assessment. Sci. Total Environ. 789, 147969.

Nia, A.S., Parashkoohi, M.G., Zamani, D.M., Afshari, H., 2024. Optimization of energy use efficiency and environmental assessment in soybean and peanut farming using the imperialist competitive algorithm. Environmental and Sustainability Indicators 100361.

Nikzad, A., Mehregan, M., 2022. Techno-economic, and environmental evaluations of a novel cogeneration system based on solar energy and cryptocurrency mining. Sol. Energy 232, 409–420.

Nikzad, A., Chahartaghi, M., Ahmadi, M.H., 2019. Technical, economic, and environmental modeling of solar water pump for irrigation of rice in Mazandaran province in Iran: a case study. J. Clean. Prod. 239, 118007.

Pascaris, A.S., Handler, R., Schelly, C., Pearce, J.M., 2021. Life cycle assessment of pasture-based agrivoltaic systems: emissions and energy use of integrated rabbit production. Cleaner and Responsible Consumption 3, 100030.

Ravilla, A., Shirkey, G., Chen, J., Jarchow, M., Stary, O., Celik, I., 2024. Techno-economic and life cycle assessment of agrivoltaic system (AVS) designs. Sci. Total Environ. 912, 169274.

REM TEC S.R.L., 2025. http://www.remtec.energy/ (Accessed: 30 July 2025).

Riaz, M.H., Imran, H., Alam, H., Alam, M.A., Butt, N.Z., 2022. Crop-specific optimization of bifacial PV arrays for agrivoltaic food-energy production: the light-productivity-factor approach. IEEE Journal of Photovoltaics 12 (2), 572–580.

Searchinger, T., Heimlich, R., Houghton, R.A., Dong, F., Elobeid, A., Fabiosa, J., Tokgoz, S., Hayes, D., Yu, T.H., 2008. Use of US croplands for biofuels increases greenhouse gases through emissions from land-use change. Science 319 (5867), 1238–1240.

SentNet S.R.L., 2025. https://www.sentnet.it/ (Accessed: 30 July 2025).

SimaPro, 2025. Software for life cycle analysis, Ver. 9.0, Pré consultants B.V.. Available at: (Accessed: 30 July 2025). https://simapro.com/plans/.

Sponagel, C., Weik, J., Feuerbacher, A., Bahrs, E., 2024. Exploring the climate change mitigation potential and regional distribution of agrivoltaics with geodata-based farm economic modelling and life cycle assessment. J. Environ. Manag. 359, 121021.

Steubing, B., Wernet, G., Reinhard, J., Bauer, C., Moreno-Ruiz, E., 2016. The ecoinvent database version 3 (part II): analyzing LCA results and comparison to version 2. Int. J. Life Cycle Assess. 21 (9), 1269–1281.

Tekie, S., Zainali, S., Zidane, T.E.K., Lu, S.M., Guezgouz, M., Zhang, J., Amaducci, S., Dupraz, C., Campana, P.E., 2025. Unraveling the crop yield response under shading conditions through the deployment of a drought index: a meta-analysis. Energy Nexus 19, 100523. https://doi.org/10.1016/j.nexus.2025.100523.

The PVSOL software, 2024. Version R8. Available at: https://pvsol.software/en/. (Accessed 30 July 2025).

Valmont Solar, 2025. https://www.valmontsolar.com/ (Accessed: 30 July 2025).

Vicente-Serrano, S.M., Beguería, S., López-Moreno, J.I., 2010. A multi-scalar drought index sensitive to global warming: the standardized precipitation evapotranspiration index – SPEI. J. Clim. 23, 1696–1718.

Wagner, M., Lask, J., Kiesel, A., Lewandowski, I., Weselek, A., Högy, P., Bauerle, A., 2023. Agrivoltaics: the environmental impacts of combining food crop cultivation and solar energy generation. Agronomy 13 (2), 299.

Weidema, B.P., Wesnæs, M.S., 1996. Data quality management for life cycle inventories—an example of using data quality indicators. J. Clean. Prod. 4 (3–4), 167–174.

Weselek, A., Ehmann, A., Zikeli, S., Lewandowski, I., Schindele, S., Högy, P., 2019. Agrophotovoltaic systems: applications, challenges, and opportunities. A review. Agronomy for sustainable development 39 (4), 35.

Wilcox, S., Marion, W., 2008. User's Manual for TMY3 Data Sets. NREL/TP-581-43156. National Renewable Energy Laboratory, Golden, CO.

Zhang, J., Wang, T., Chang, Y., Liu, B., 2023. A sustainable development pattern integrating data centers and pasture-based agrivoltaic systems for ecologically fragile areas. Resour. Conserv. Recycl. 188, 106684.

Zidane, T.E.K., Zainali, S., Bellone, Y., Guezgouz, M., Khosravi, A., Lu, S.M., Tekie, S., Amaducci, S., Campana, P.E., 2025. Economic evaluation of one-axis, vertical, and elevated agrivoltaic systems across Europe: a Monte Carlo analysis. Appl. Energy 391, 125826.